Agarose-based Gel Electrolytes for Sustainable Primary and Secondary Zinc-Air Batteries

Original
Agarose-based Gel Electrolytes for Sustainable Primary and Secondary Zinc-Air Batteries / García-Gaitán, Estibaliz; Carmen Morant-Miñana, María; Frattini, Domenico; Maddalena, Lorenza; Fina, Alberto; Gerbaldi, Claudio; Cantero, Igor; Ortiz-Vitoriano, Nagore. - In: CHEMICAL ENGINEERING JOURNAL. - ISSN 1385-8947. - STAMPA. - 472:(2023), pp. 1-17. [10.1016/j.cej.2023.144870]

Publisher:
Elsevier

Published
DOI:10.1016/j.cej.2023.144870

Agarose-Based Gel Electrolytes for Sustainable Primary and Secondary Zinc-Air Batteries

Estibaliz García-Gaitán [a, b, c], *María Carmen Morant-Miñana* [a], *Domenico Frattini* [a], *Lorenza Maddalena* [d], *Alberto Fina* [d], *Claudio Gerbaldi* [e, f], *Igor Cantero* [c], *and Nagore Ortiz-Vitoriano* [a, g, *]

[a] Centre for Cooperative Research on Alternative Energies (CIC energiGUNE), Basque Research and Technology Alliance (BRTA), Alava Technology Park, Albert Einstein 48, 01510, Vitoria-Gasteiz, Spain.
[b] University of the Basque Country (UPV/EHU), Barrio Sarriena s/n, 48940, Leioa, Spain.
[c] CEGASA Energía SLU, Álava Technology Park, Marie Curie 1, 01510, Miñano, Spain.
[d] Department of Applied Science and Technology (DISAT), Politecnico di Torino, Alessandria Campus, Viale Teresa Michel 5, 15121, Alessandria, Italy.
[e] Group for Applied Materials and Electrochemistry (GAME Lab), Department of Applied Science and Technology (DISAT), Politecnico di Torino, Corso Duca degli Abruzzi 24, 10129, Turin, Italy.
[f] National Reference Center for Electrochemical Energy Storage (GISEL)-INSTM, Florence, Italy.
[g] Ikerbasque, Basque Foundation for Science, María Díaz de Haro 3, 48013, Bilbao, Spain.
* Corresponding Author, E-mail: nortiz@cicenergigune.com

Abstract Present Zn-air batteries (ZABs) are based on concentrated alkaline liquid electrolytes, with high ionic conductivity, but suffer from leakage, evaporation, and carbonate precipitation due to the semi-open characteristic of these systems. To overcome these issues, gel polymer electrolytes (GPE), based on naturally occurring biopolymers, arise as a green option to overcome the above-mentioned limitations. In this work, a novel GPE based on pure agarose from seaweed is presented as a smart alternative to liquid (adsorbed on a separator) and gel electrolytes (based on synthetic polymers). The innovative synthesis method described can directly encapsulate concentrated KOH liquid electrolytes into an agarose matrix in one-pot; the process requiring approx. 10 min. The unique gel developed in this work, with 2 wt.% agarose and 8 M KOH electrolyte, presents the best compromise between physicochemical and electrochemical properties, at lab scale. The characterization results revealed an outstanding ionic conductivity of 0.45±0.05 S cm^{-1}, ≈100% water retention up to 200-250 h, retarded Zn self-corrosion up to 30 days (symmetric cell under open circuit), average Zn utilization >70-80% in primary ZABs in the range 1-20 mA cm^{-2} with peaks of ≈96%. In secondary ZABs the gel electrolyte presents high round-trip efficiency and improved cyclability at high areal capacities, under soft and severe cycling conditions, never tested before. This agarose gel represents a potential benchmark for future development of GPE-based ZABs for stationary applications.

Keywords: gel polymer electrolyte, agarose, natural biopolymer, solid-state, zinc-air battery

1. Introduction

In the development of batteries with high energy density, safety, sustainability, and rechargeability at very low cost, rechargeable zinc-air batteries (ZABs) [1] arise as a great opportunity due to their semi-open character, the use of inexhaustible oxygen from air, providing a high theoretical energy density (1350 Wh kg^{-1}, theoretical cell voltage of 1.66 V [2]), so that are regarded as one of the best candidates to complement standard lithium-ion batteries (LIBs). In recent reports [3,4] environmental and economical assessment conclude that the costs and impacts of ZABs are potentially lower than other technologies like lead acid, Na-S, Ni-Cd, LIBs, and redox flow if the cyclability is improved, and have attracted therefore the utmost attention due to the cheap materials involved, environmental friendliness, and safe operation [5,6] that can be used in hybrid storage solutions to exploit the high energy density and low cost of ZAB in synergy with the durability and rate capability of LIB. For their practical use, challenges such as low Zn utilization and lifetime for primary, short cycle life and low power density for secondary ZABs have not been solved yet. These issues involve all the components, and particularly the electrolyte system plays an essential role in the performance because it is the medium for the bidirectional ionic migration [7].

In ZABs, KOH 6-8 M concentrated solutions are the most commonly used liquid electrolytes due to their optimal viscosity, conductivity, and possibility to dissolve Zn salts (e.g., zinc acetate) to pre-saturate the electrolyte with zinc ion, however, they present several challenges such as the precipitation of zinc-based compounds (e.g., ZnO, $Zn(OH)_2$) [8], vulnerability to CO_2/O_2 crossover, susceptibility to evaporation or leakages, and hydrogen evolution reaction (HER) [9,10]. Carbonate precipitation caused by atmospheric CO_2 and leakage and/or evaporation of the liquid electrolyte are the two main drawbacks and ZABs' barriers to challenge LIBs [6]. To alleviate these disadvantages, the substitution of the liquid electrolyte by a soft gel polymer electrolyte (GPE) [11–14], is particularly useful for flexible applications [15,16]. The use of GPEs minimizes the flooding of the electrodes, evaporation, leakage, and corrosion problems, while possessing sufficiently high ionic conductivity, demonstrated adaptability to extreme temperatures [17,18], but often weak mechanical strength [19,20]. Currently, GPEs with high ionic conductivities and good mechanical properties are obtained from (crosslinked) synthetic polymers, like poly(vinyl alcohol) (PVA), poly(acrylic acid) (PAA), poly(acryl amide) (PAM), and poly(ethylene oxide) (PEO). However, the use of naturally occurring biopolymers (e.g., cellulose, agars, gelatins, starch-based, chitosan, etc.) is rapidly gaining importance [21] to avoid petroleum-based plastics in electrochemical storage devices [22] and in ZABs [23–26]. Many reports [27,28] have already established the benefits of naturally occurring biopolymers as substitutes of petrochemical plastics in terms of greenhouse gas and fossil fuel savings, lower environmental impacts, and non-competitive nature to food and land-use, especially if algal-derived [29,30].

Among others, red seaweeds (Rhodophyceae) contain sulphated galactans as the main structural materials of cell walls and intercellular matrices, known as Agar, a mix of agaropectin (containing the sulphated groups), and agarose (the main component giving jellification) [31]. This extraordinary jellification is due to the 1,3-linked β-d-galactopyranose and 1,4-linked 3,6-anhydro-α-l-galactopyranose blocks constituting the agarose biopolymer chain, including ≈400 repeating units. Agarose gels are considered reversible physical gels forming a 3D structure of channels commonly employed for proteins' separation.

So far, previous examples of the specific use of agarose and/or agar in energy storage devices can be found in the literature. Agar has been employed as electrolyte mixed with PVA [32], water soluble graphene oxide [33] or sorbitol [34], as a component of electrochromic devices [35], as anode additive [36,37], and electrode binder [19,38,39]. Agarose has been used as gel electrolyte with NaCl for supercapacitors and the mechanical and conductivity properties of agarose matrices in the presence of KOH (1 M) have been described by Moon et al. [40], and Ueno et al. [41], respectively. Further examples of agarose as solid-state electrolyte (SSE) have been reported in other technologies such as Mg-air [33], Li-ion [42], Al-air [43], supercapacitor [44], or zinc-ion batteries [45]. In ZABs, agarose has been often reported as binder for electrodes. Mohamad et al. [46] reported agar as binder for the anodes, prepared by mixing Zn powder and agar paste with 0.2, 0.4 and 0.6 M KOH. Han et al. [47] reported a Fe-N/C catalyst derived from the pyrolysis of agarose in the presence of urea and α-Fe_2O_3 nanoparticles as cathode. Similarly, Zhang et al. [48] reported the use of an agarose gel to prepare bimetallic (iron and cobalt) nitrogen doped carbon composites (FeCo-NC). Jose et al. [49] reported the use of an agarose-based gel as binder, mixed with $Mn(NO_3)_2$ and $NaNO_3$, for a gelled cathode. Kim et al. [50] reported agarose as a binder for electrode to form a gel for the electrodeposition of MnO_2 and Co_3O_4 onto 3D porous nickel foam as support.

The scenario is that many of the agarose-based gel electrolytes and applications reported in previous literature are used in different intercalation-based storage devices. In this work we focus on ZAB that is a conversion-based device, relying on the chemical reduction and evolution reactions of oxygen (ORR/OER). Hence, although agarose is used as the polymer matrix material, the conduction mechanism is different, and less examples of sustainable GPEs for this technology are reported. Agarose gel electrolytes are an excellent choice for zinc-air batteries due to their enhanced stability, safety, mechanical integrity, controlled ion transport, longer shelf life, and adequate ionic conductivity. The solid or semi-solid consistency of gel electrolytes reduces the risk of leakage and evaporation, ensuring the battery's safety and longevity by providing mechanical support, preserving the battery's structural integrity. Unlike liquid electrolytes, gels are less prone to leakage, minimizing spills, hazardous chemical exposure, and preventing short circuits. Additionally, gel electrolytes can be designed with specific pore sizes or structures to regulate ion movement, enabling better control over ion diffusion; thus, improving efficiency. They also present an extended life because the solid or semi-solid nature preserves the electrolyte composition and reduces degradation during storage. Although gel electrolytes may exhibit slightly lower ionic conductivity compared to liquid electrolytes, the numerous advantages make them highly preferable in various applications, where the benefits outweigh the lower ionic conductivity.

In this work, we report a novel and comprehensive study about the encapsulation of concentrated KOH solutions in the agarose biopolymer matrix that avoids the direct contact with the Zn anode, and therefore retarding Zn corrosion in presence of high KOH concentration because the larger time needed for electrolyte release avoids the surface corrosion of the anode and allows for % of Zn utilization close to 100% which are rarely reported in the literature.

In addition, the synthesis method and the liquid electrolyte embedding strategy are extremely important to determine the final properties of the gel [51]. In ZAB technology, several biopolymer-based electrolytes such as starch, PVA, PAA, cellulose, sago, and agarose/agar have been prepared by not direct (e.g., not one-pot) methods, requiring multi-steps, hence time consuming, potentially not industrially scalable [51]. A new approach for the use of agarose as GPE in ZABs is therefore required to improve properties and performance.

Unlike the actual state-of-the-art, in this work, agarose is directly dissolved in a KOH solution (6 or 8 M), and the total process for obtaining a ready-to-use gel is less than 10 minutes. The agarose matrix does not form granules during the gelation process, providing homogeneous smooth interfaces between the gel electrolyte and both electrodes. The successful encapsulation of concentrated KOH solutions reported here is embodied by a new GPE with excellent balance between flexibility, stiffness, compression resistance, and ionic conductivity, obtaining unprecedented properties for excellent electrolyte retention, electrochemical stability, and therefore excellent performance in ZABs, with a zinc utilization >96% in primary batteries and, remarkably, secondary batteries based on GPE with longer operating time and cyclability, demonstrated at high areal capacities never investigated before [52].

2. Materials and Methods

2.1. Materials and electrolyte/electrodes

For gel electrolyte preparation, agarose (Low EEO, electrophoresis grade, Scharlab, Spain), agar-agar (Agar for microbiology, Sigma-Aldrich, Germany), xanthan (Xanthan gum from Xanthomonas campestris, Sigma-Aldrich, Germany) powders, and κ-carrageenan (Kappa-Carrageenan; Acros Organics, Belgium), potassium hydroxide (KOH, pellets, extra pure grade, Scharlab, Spain), and distilled water (type II analytical grade, <1 µS cm^{-1}, ECOMATIC, Wasserlab, Spain) were used. All chemicals were used as received without further purification. For full cells, anode is obtained by mixing zinc powder (Zn >98%, CEGASA Energía SLU, Spain) and a 45 wt.% KOH solution to form a paste (Zn mass loading approx. 65%). The cathode for primary cells is a mixture of MnO_2, carbon conductive additive, and poly(tetrafluoroethylene) (PTFE) binder, kindly provided by CEGASA, Spain. For secondary cells, this primary catalyst is purposefully mixed with nickel cobalt oxide (NCO, $NiCo_2O_4$, >99%, Sigma-Aldrich, Germany), and ethanol in a 1:1:1 mass ratio to obtain a paste.

2.2. Ionic conductivity and FTIR measurements

The ionic conductivity was measured by electrochemical impedance spectroscopy (EIS), using a Solartron 1260A Impedance/Gain-Phase Analyzer (Ametek Inc., Berwyn, PA, United States). The materials were tested in a frequency range from 10 MHz to 100 Hz applying 50 mV as polarization amplitude. The gel electrolytes were punched with a 3 mm diameter punch tool and assembled inside a coin cell (type CR2032) with a Teflon sheet spacer, where a 3 mm diameter hole is used to place the sample. For ionic conductivity measurements as function of temperature, a temperature-controlled incubator (KB-23, Binder Inc., Bohemia, NY, United States) was used. The average of, at least, three replicated measures is reported. The value for the electrolyte resistance is obtained from the intercept of the Nyquist plot with the X axis. The ionic conductivity (σ) of the membrane is then calculated using the following equation:

$$\sigma = \frac{t}{A} \cdot \frac{1}{R} \qquad (1)$$

where t, A, and R are the thickness, area, and resistance of the membrane, respectively. The thickness of the membrane was measured after performing the EIS measurements. The ionic conductivity has been used for the estimation of the activation energy (E_a) − related to the energy required by the ion to release from its bond and migrate to another coordinating site through the conduction process − employing Arrhenius plot of ln σ against 1000/T. Arrhenius plot is obtained using the following equation:

$$Ln\sigma = (-\frac{E_a}{R})\frac{1}{T} + LnA \qquad (2)$$

being E_a the activation energy in J mol^{-1}, R ideal gas constant (8.314 J mol^{-1} K^{-1}), T is the temperature in K, A the Arrhenius constant.

FTIR measurements were carried out running a Vertex 70 Microscope from Bruker (Billerica, MA, United States). All the sample spectra of materials were recorded under argon flow, corrected for the background, and collected in the wavelength range 4000–400 cm^{-1} as average of 64 repeated scans.

2.3. Relative weight losses and flexibility test

The materials' weight losses were measured by using a precision scale and a temperature-controlled incubator (KB-23, Binder Inc., Bohemia, NY, United States) at 30±1ºC and environmental relative humidity 40±5%. Three replicated samples for each electrolyte were poured into a vial tapped by an aluminum foil with tiny holes and weighted at the initial time. The weight of each vial was checked daily for a total of 21 days (approx. 500 h), and average relative weights, R_w were calculated using the following equation:

$$R_w = \frac{m_f \cdot 100}{m_i} \tag{3}$$

where m_f, and m_i are final mass of each day and initial mass, respectively.

The bending angle of material (2 wt.% agarose in 8 M KOH) was simply measured by placing specimen on lab beakers/stirrers with different radii, from 5 cm to 0.5 cm. The arc angles were measured with a manual goniometer.

2.4. Compression tests (till failure and hysteresis)

Stress [kPa] vs Compression strain [%] curves were collected by means of Instron 5966 (Instron engineering Corp., Norwood, MA, United States) equipped with a 2kN cell applying a 5 mm min^{-1} compression strain rate. The hydrogel samples (cylindrical, diameter 24 mm and heights 2.4 ± 0.1 mm for 6 M KOH and 2.7± 0.3 mm for 8 M KOH) were placed between the self-leveling plates, with protective polyethylene sheets to avoid plates corrosion, and tested until failure occurred. For the hysteresis test, the loading and unloading cycles (5 cycles) were performed at a constant compression/decompression rate (5 mm min^{-1}) and up to a compression strain of 15%. The elastic modulus was calculated as the slope of the tangent line to compression stress/strain curve in the range 0-2% of strain. For each sample, a minimum of three measurements is conducted and the most representative curves are reported.

2.5. Cell assembly and electrochemical measurements

Full cells were assembled using an in-house design, consisting of a circular Teflon body with compartments for components. Anode paste is dripped in a circular cavity of 13 mm. Upon it, an agarose gel disk of 24 mm in diameter is placed. Then, for primary cells, approx. 250 mg of cathode powder covered it, whereas for secondary cells the MnO_2/NCO paste was pressed on a Ni mesh and dried in oven at 60 ºC overnight. The assembly is completed by Ni-based current collectors as electrical contacts. A Teflon cap, with two aeration holes, closes the cell. Sealing is ensured by pression thanks to an O-ring and two bolts. For symmetric cells, the same in-house design was used but the Teflon cap had no aeration holes and presents a circular cavity of 13 mm designed to place approx. the same amount of Zn paste on both sides of the gel electrolyte. Both sides are thus not exposed to air.

The anode area (1.33 cm^2) is used to calculate current densities in all experiments; Zn extractions, specific capacities, and all the other metrics [53], are normalized by using the theoretical capacity of Zn (819.73 mAh g^{-1}), and the masses indicated for each cell. For primary cells, metrics were calculated according to the following equations:

$$Zn_{utilization} = \frac{C_{cell}}{m_{Zn} \cdot 819.73} \cdot 100 \qquad (4)$$

$$f_{Zn} = \frac{m_{Zn}}{m_{anode} + m_{gel} + m_{cathode}} \qquad (5)$$

$$E_{density} = \frac{Zn_{utilization}}{100} \cdot 819.73 \cdot f_{Zn} \cdot V_{avg} \qquad (6)$$

Where $Zn_{utilization}$ is the percentage of discharged zinc vs. available zinc in the primary cell, C_{cell} is the total capacity delivered by the primary cell, m_{Zn} is the mass of active zinc, f_{Zn} is the zinc weight fraction in the cell, $E_{density}$ is the gravimetric energy density of the cell, m_{anode}, m_{gel}, and $m_{cathode}$ are the total mass of anode, gel, and cathode used in the cell, and V_{avg} is the average discharge voltage of the cell. For secondary cells, metrics were calculated according to the following equations:

$$DoD_c = \frac{1.33 \cdot j \cdot t_{dis}}{m_{Zn} \cdot 819.73} \cdot 100 \qquad (7)$$

$$DoD_{tot} = n_c \cdot DoD_c \qquad (8)$$

$$RTE = \frac{V_{avg}}{V_{ch}} \cdot 100 \qquad (9)$$

$$E_{density} = \frac{DoD_{tot}}{100} \cdot 819.73 \cdot f_{Zn} \cdot V_{avg} \qquad (10)$$

Where 1.33 cm^2 is the anode area in this work used for normalization, DoD_c and DoD_{tot} are the depth of discharge per cycle and total (cumulative), respectively, j is the current density, t_{dis} is the discharge time per cycle, n_c is the number of cycles, RTE is the round-trip efficiency (voltaic), and V_{ch} is the average charge voltage.

Galvanostatic experiments were performed on a BCS 815 potentiostat (BioLogic, Seyssinet-Pariset, France) to determine the electrochemical behavior of agarose biopolymer gel electrolyte jellified in KOH solutions. Tests were conducted in constant current (CC) mode. For primary cells, the current density applied was from 1 to 30 mA cm^{-2}, limiting the cutoff voltage to 0.8 V. For secondary cells, symmetric cycles (i.e., same discharge/charge time) and current densities ranging between 1, 2, 5, and 10 mA cm^{-2} were applied at various cycling times, to span different areal capacities, from 1.67 to 60 mAh cm^{-2} [54]. Cutoff voltages for discharge and charge were 0.6 V and 2.2 V, respectively. For symmetric cells, open circuit voltage (OCV) was monitored over time up to 1400 h (approx. 60 days), and impedance response (EIS) was checked every 8 h in a frequency range of 300 kHz to 100 mHz, and 10 mV as polarization amplitude using a VMP3 potentiostat (BioLogic, Seyssinet-Pariset, France). Symmetric cells cycling was carried out at 2 mA cm^{-2} for 12 h per cycle.

3. Results and Discussion

3.1. Preparation of the biopolymer gel electrolytes

The biopolymer gel electrolyte was obtained by mixing the desired amount of biopolymer in 25 mL of KOH solution at different molar concentrations to achieve the desired weight percentage of agarose. After reaching a homogeneous dispersion, the mixture was uniformly and rapidly heated up to 100-120 ºC for few minutes, under continuous shaking as it is shown in **Figure 1**.

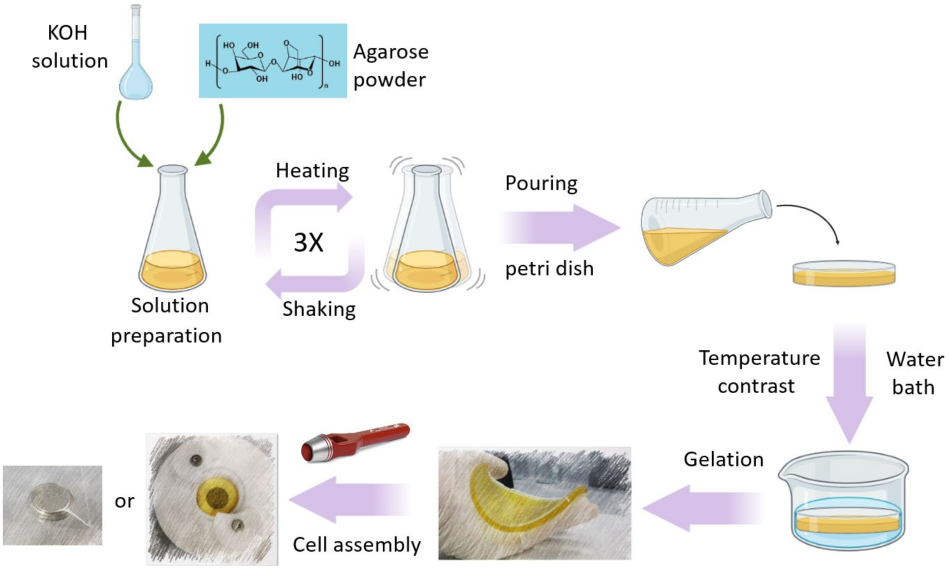

Figure 1. Schematic diagram of the synthesis of the agarose and KOH gel electrolyte.

Subsequently, the mixture was quickly poured into a petri dish and quenched by immersion in a water bath until the complete jellification. The gel time formation depended on the KOH concentration. The jellifying process of the gels containing a KOH concentration lower than 8 M, started at room temperature, and finished requiring one hour of curing in the oven. The selected temperature, 36 ºC, is the jelling point of the agarose. On the contrary, samples containing 8 or 10 M KOH solutions formed a gel after a few seconds. A summary with the experimental conditions for the obtention of the 2 wt.% of agarose gels is listed in **Table 1**.

Table 1. Synthesis conditions of agarose-based biopolymer gels.

KOH concentration [M]	Heating time [min]	Water cooling [Yes/No]	Curing Temperature [ºC]	Curing time [h]	Jellifying time [h]
2	4	Yes	36	1	24
4	4	Yes	36	1	15
6	5	Yes	36	1	5.5
8	5.5	Yes	(a)	0	0.01
10	4	No	(a)	0	0.01

(a) Not needed

Indeed, gels with 2 wt.% agarose present a jellification time (**Table 1**) inversely proportional to the KOH molar concentration, being 1 day for 2 M KOH and requiring in some cases a curing step, down to few minutes for 10 M KOH, without any curing. A very short, quite instant, jellification limits the processability of the gels, hence the gels at 2 wt.% agarose, KOH 6 M and 8 M, have been selected for further study. As it is shown in **Table 1**, the higher the concentration of KOH solution, the faster the jellifying process and the curing step is no longer required. The gelation mechanism of agarose still remains a matter of controversy and it is not clear yet if the mechanism is spinodal decomposition or nucleation and growth [55]. However, according to the most accredited theory, the gelation mechanism is explained for the formation of intramolecular and intermolecular hydrogen bonding occurring between the D-galactose and 3,6-anhydro-alpha-L-galactopyranose molecules. This association results in a cage effect, which leads to the lowest energy state of electrons of the lone pairs of ring oxygen atoms of the anhydro-L-galactopuranosyl residues. The conformation adopts a tetrahedral distribution and, therefore, attracts not only each other but also water molecules due to hydrogen bonding [56]. In presence of NaOH (ca. 2.5 M, 50-60 °C and 0.5-1 h of treatment), it is described by some authors a reinforcement of the gel strength, and this is correlated with a decrease in the yield of sulfate molecules, the increase of the 3,6-anhydrogalactose, and a negligible change in the O-methyl and pyruvic acid contents [57]. Based on this, we hypothesize that the mechanism behind the rapid gelation with increasing KOH concentration is due to the higher hydrolysis of the sulfate content and simultaneous formation of numerous bonds within the 3,6-anhydrogalactose blocks, thereby improving the gelling properties [58].

3.2. Characterization results

3.2.1. FTIR

In order to verify the synthesis procedure, and that the electrolyte is embedded in the biopolymer matrix, the molecular structure of the 8 M KOH gel was checked and compared to agarose powder precursors and 8 M KOH liquid electrolyte (**Figure 2**). FTIR spectra of gel 6 M KOH are reported in **Figure S1**.

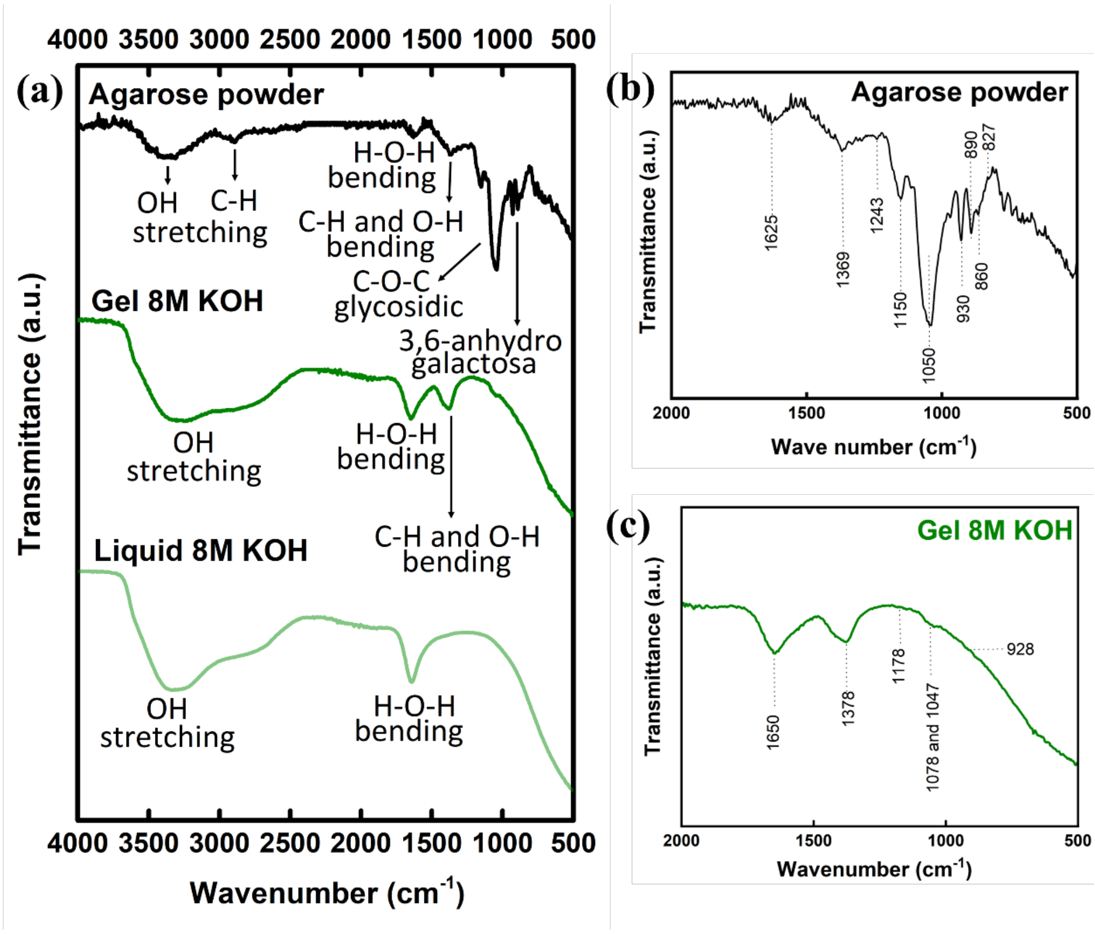

Figure 2. a) FTIR spectra of agarose powder, agarose gel with 8 M KOH electrolyte, and liquid electrolyte 8 M KOH; b) Inset of FTIR spectrum of agarose powder; c) Inset of FTIR spectrum of agarose gel 6 M KOH.

In **Figure 2a** the characteristic absorption bands of the spectra, with the corresponding functional groups are reported, and together with literature references for the three samples in **Table S1**. The agarose powder spectrum shows a broad and relatively weak absorption band between 3680-3050 cm^{-1} and centered approx. at 3365 cm^{-1} that is ascribed to stretching mode of the hydroxyl group of water molecules (agarose powder is hygroscopic) [59,60]; the sharp and medium intensity band at 1045 cm^{-1} coupled with a weak band at 1156 cm^{-1}, are both assigned to the vibration mode of C–O–C bridge of glycosidic linkage [59,60], while the band at 932 cm^{-1} reflects the vibration mode of the C–O–C bridge of the 3,6-anhydrogalactose unit [61,62]. The other secondary bands for agarose powder (see **Figure 2b**) are listed in **Table S1**. For the gel 8 M KOH, three characteristic adsorption bands are visible. The first two, at 3272 and 1645 cm^{-1} are the same as the liquid 8 M KOH [60,63,64]. Comparing the values of the O-H stretching vibration bands in **Table S1**, it is possible to interpret the small shift toward lower wavenumbers, from 3320 cm^{-1} of the liquid to the 3272 cm^{-1} of the gel as an effect of the formation of strong hydrogen bonds between the water molecules and the biopolymer matrix, especially if the polymer is hydrophilic [65], as in the case of agarose. The third one at 1378 cm^{-1} is new, absent in the liquid 8 M KOH and not clearly visible, or very weak, in agarose powder, and represents the overlapped bending modes of C-H and O-H (hydroxyl groups not related to water) bonds [61,62]. The appearance of this peak could be ascribed to the strong hydrogen bonds formed inside the gel due to the reaction between water, KOH, and agarose functional groups [58,61,62]. Finally, a residual signal around 1000-1180 cm^{-1} can be noted in the spectrum of gel (**Figure 2c**) that is ascribed to the strong C-O-C glycosidic band from agarose powder. For liquid 8 M KOH, the spectrum is almost identical to that of water, with only two absorption bands detected. The first band at 3320 cm^{-1} corresponds to the O-H stretching band [59,60], and the band at 1645 cm^{-1} is ascribed to bending mode of H-O-H [60,63,64].

3.2.2. Ionic conductivity

Among the different parameters to be considered for developing GPEs, ionic conductivity is crucial because it influences the ohmic resistance of the battery and determines the ion mobility inside the gel [7]. Hence, the effect of the KOH molar concentration in the range between 2 and 10 M and the amount of biopolymer (from 0.5 wt.% to 3 wt.%) on the GPE ionic conductivity was measured and the results are summarized in **Figure 3a and 3b,** respectively.

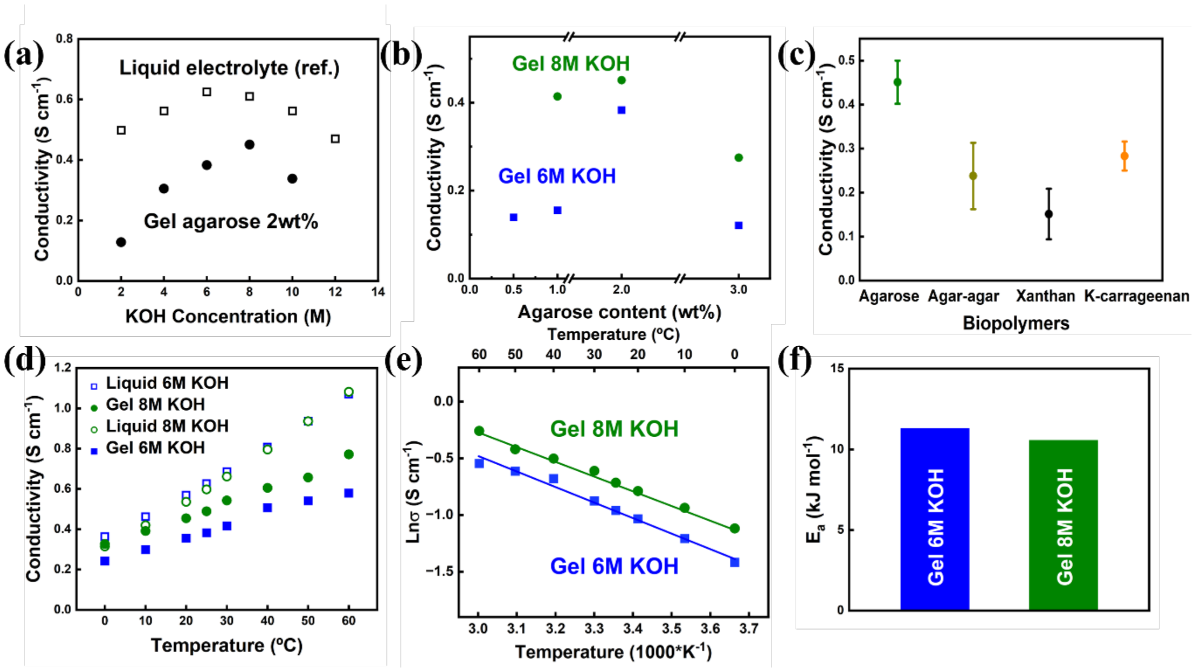

Figure 3. Ionic conductivity of alkaline biopolymer gels as a function of: (a) KOH concentration, (b) agarose content, (c) biopolymer type, (all measures are at room temperature) and (d) temperature; (e) Arrhenius plot showing ionic conductivity vs. temperature for liquid and gel electrolytes at KOH 6 M and 8 M, and (f) activation energy of gel 6 M KOH and gel 8 M KOH. Data for liquid electrolytes in Figure 3a and 3d are taken from Gilliam et al. [66].

In **Figure 3a**, the ionic behavior of agarose gel electrolytes was determined and compared to reference KOH liquid electrolyte conductivities at different KOH concentrations as from Gilliam et al. [66]. The agarose gel possesses a very high ionic conductivity, just slightly lower than KOH liquid electrolytes and in the same order of magnitude. The gels with 6 M and 8 M KOH present the highest ionic conductivity and therefore were selected for further studies. In **Figure 3b**, the initial 2 wt.% agarose content, for the 6 M and 8 M KOH concentrations, was varied to check the effect on ionic conductivity. The gels at 2 wt.% possess the highest ionic conductivity for both KOH concentrations. An interesting comparison is proposed in **Figure 3c**, where, by using the 8 M KOH solution, 2 wt.% of biopolymer content, and the same jellification protocol used for agarose, the ionic conductivity of gels with other natural biopolymers is compared. Although being in the same order of magnitude, the conductivity values of gels using agar-agar, xanthan, and κ-carrageenan are lower than agarose, thus proving the benefits of agarose. This result also demonstrates that this synthesis method can be applied with no substantial modifications also to other biopolymers, such as Xanthan (0.151 S cm^{-1}) or κ-carrageenan (0.283 S cm^{-1}) (**Figure 3c**) achieving higher ionic capacities than those reported in the literature for similar Xanthan/8 M KOH and κ-carrageenan/8 M KOH gels [33].

A useful information for prospective industrial development toward market, is related to gel ionic conductivity behavior as function of temperature. In **Figure 3d** the ionic conductivity trends are shown in the 0 – 60 ºC range and compared to data for liquid electrolytes as available from Gilliam et al. [66], viz. the common operational temperature range for a commercial battery. To complement this information, a brief thermal characterization of pristine and an aged gel 8 M KOH is reported and discussed in the supplementary information (see **Figure S2**). Ionic conductivity values of both liquid and gel electrolytes increase with the temperature as expected [66]. However, in an alkaline gel, the conduction mechanism is different because, dissimilarly to proton hopping mechanism, hydroxyl anions are conducted via hyper-coordinated and per-solvated complexes of OH^- by four H_2O molecules. When this $[OH(H_2O)_4]^-$ complex gets close to a new water molecule, the coordinated OH^- establishes a H-bond with the water molecule and takes over an H^+ to form a new OH^- that carries the negative charge, and pass it again to other solvent molecule [67]. A temperature increment expands the pores of the biopolymer matrix, redistributing the liquid electrolyte in the gel, hence increasing ionic conductivity without causing evaporation [68].

The Arrhenius plot and activation energies of the gels at 2 wt.% agarose with 6 M and 8 M KOH are shown in **Figure 3e and f,** respectively. The linear fits of conductivity data are reported in **Figure 3e**, showing a good regression for both gels (R^2 is 0.985 for gel 6 M KOH, while is 0.995 for gel 8 M KOH). The activation energy values calculated are compared in **Figure 3f**, showing E_a 11.32 kJ mol^{-1} for the gel 6 M KOH whereas for the gel 8 M KOH is 10.57 kJ mol^{-1}. This lower value of E_a for the gel 8 M KOH, and the superior ionic conductivity, further supports that the involved ions could transport/diffuse easier because less energy is required, compared to the gel 6 M KOH. For instance, **Table 2** compares the E_a reported for other gel electrolytes based on natural/synthetic polymers.

Table 2. Comparison of E_a ranges for GPEs based on synthetic or natural polymers.

Gel type	E_a [kJ mol^{-1}]	Refs.
Agarose 8 M KOH	**10.57**	**This work**
Agarose 6 M KOH	**11.32**	**This work**
QAFC with/without GO	8.40-16.30	[69]
Chitosan with NH_4SCN	13.40-14.30	[70]
κ-carrageenan with NH_4NO_3	6.07-10.13	[71]
PVA-KOH	22.00-28.00	[72]

PVA-KOH	13.50-14.00	[73]
PVA-KOH	15.44-20.26	[74]
PVA-KOH	3.00-15.00	[75,76]

Zhang et al. [69] reported E_a in the range of 8.4 to 16.3 kJ mol^{-1} for a quaternary ammonium functionalized cellulose (QAFC) with/without graphene oxide; Shukur et al. [70] further reported values of E_a between 13.4 and 14.3 kJ mol^{-1} for chitosan-based solid biopolymer electrolytes containing ammonium thiocyanate (NH_4SCN) with glycerol as plasticizer, and Rudhziah et al. [71] reported values of approx. 6.07 and 10.13 kJ mol^{-1} for a gel electrolyte based on seaweed κ-carrageenan with NH_4NO_3. In all cases the ionic conductivities were in the range of few mS cm^{-1}. Similarly, for gel electrolytes based on synthetic polymers, different activation energy values are available for PVA-based gel. For a PVA-KOH polymer electrolyte with a ionic conductivity of 10^{-3} S cm^{-1} at room temperature, Lewandowski et al. [72] reported E_a in the range of 28 and 22 kJ mol^{-1} whereas Mohamad et al. [73] reported an E_a of approx. 14-13.5 kJ mol^{-1}; Santos et al. [74] described E_a in the range of approx. 15.44 to 20.26 kJ mol^{-1} for PVA-KOH electrolyte with a high ionic conductivity of 0.34 S cm^{-1} and Yang et al. [75,76] disclosed E_a in the range of 3–15 kJ mol^{-1} for PVA-KOH gel electrolyte with ionic conductivity ranging between 47-61 mS cm^{-1}. Therefore, the gels developed in this work present both favorable ionic conductivity (0.383 and 0.451 S cm^{-1} for 6 M KOH and 8 M KOH gels) and lower activation energy (13.29 kJ mol^{-1} for the gel 6 M KOH and 10.57 kJ mol^{-1} for the gel 8 M KOH.) compared to gel based on synthetic (from 10^{-3} S cm^{-1} to 0.34 S cm^{-1}; and from 3 to 28 kJ mol^{-1}) and/or natural (from $0.141 \cdot 10^{-4}$ S cm^{-1} to 0.042 S cm^{-1}; from 8.4 to 16.3 kJ mol^{-1}) biopolymers in the literature.

Moreover, the synthesis method is also important to evaluate the overall benefits of the agarose gel developed in this work. For instance, some of the methods reported to synthesize agarose/agar gels for ZABs [37,77,78] consist of first dissolving the agarose powder in water at high temperature (90 ºC), requiring at least 30 minutes, and then further soaking of the obtained neutral gel in an alkaline media (KOH or KOH/$ZnCl_2$) for several hours. Very recently, Yang et al. [77], the reported method for agar-PVA/GO gel is more complex and longer, as agar is dissolved in a PVA/GO solution at 95 ºC, but the gelation requires two freezing/thawing (-20 °C/RT) cycles. This method requires approx. 9 h for obtaining the final gel. Additional steps prolong and complicate the synthesis. In another recent work [78], before the jellification of agar, the biopolymer dissolution is injected into a melamine foam and cooled down to RT for 1 h and then soaked for 12 h in the liquid electrolyte. In this case, the discharge capacity reported was given by area instead of Zn mass, and the applied current density was 2 mA cm^{-2}, but the performances were not good enough. The synthesis method developed here is one-pot and can synthetize a highly performing gel in few minutes instead of hours, thus being very convenient, time saving, and providing superior gel properties.

3.2.3. Electrolyte retention and weight losses

One of the key considerations to replace liquid electrolytes soaked in standard separators in ZABs is due to their low stability and durability once exposed to air [79]. Indeed, liquid electrolytes in technologies open to air tend to evaporate and if added in excessive amounts, could cause a leakage instead. This leads to safety concerns due to the release of corrosive media. To quantify this aspect, the 8 M and 6 M KOH gels have been tested for liquid retention against a glass fiber separator soaked with 8 M KOH. The relative weight *vs.* time measurement is presented in the supporting **Figure S3**. The agarose biopolymer matrix can retain electrolyte for longer time when using a KOH concentration of 8 M: it is observed that the gel can retain water without substantial weight change up to 240 h (i.e., 10 days) and, after 528 hours (22 days), only loses 26% of its initial weight. On the contrary, the gel 6 M KOH shows poorer retention, and a noticeable weight loss (≈10%) after few days, which remains stable until approximately 240 h (10 days). At this point, the material is not capable of retaining the liquid, causing a strong drop in weight, almost 40% of weight loss (22 days). This effect is directly related to the microstructure of the agarose gel since the higher the KOH concentration the higher the density of the network and the lower the water release observed due to the decreased pore size [58].

Nonetheless, the results obtained with the glass fiber separator show the importance of embedding the liquid electrolyte in a polymer matrix to ensure a longer battery life. Indeed, the glass fiber cannot retain the liquid electrolyte, and after 24 h the relative weight loss is already ≈40%. After 10 days (240 h), the weight loss is almost 55%, and then reaches a constant value. This is due to the precipitation of KOH crystals, when all the liquid is evaporated, and the residual weight represents the dried glass fiber. This means that the gel offers not only the possibility to avoid evaporation and leakage, but also to “immobilize” larger excesses of electrolyte by using just 2 wt.% of biopolymer matrix instead of around 40 wt.% of inactive separator. In **Table 3** a brief comparison with examples from the literature is reported.

Table 3. Comparison of weight losses for different GPEs.

Gel type	Time [h]	Weight loss [%]	Refs.
Agarose 8 M KOH	**528**	**25.95**	**This work**

Agarose 6 M KOH	**528**	**39.47**	**This work**
Agar-PVA-GO	24	41.80	[77]
Agar-melamine foam	24	58.00	[78]
Starch 6 M KOH	18	16.00	[80]
PVA 1.7 M KOH	72	40.60	[81]
PVA-SiO_2 5 wt.% 6 M KOH	40	37.60	[82]
PANa 6 M KOH	185	2.70	[83]

Comparing with the literature it should be considered that, for the data reported, humidity and temperature of tests may vary, however, embedding the liquid electrolyte in an agarose biopolymer matrix, as shown in this work, greatly retard the time needed for electrolyte evaporation. Other recently reported agar-based gels present liquid electrolyte retention of 58.2% [77] and 42% [78] after 24 h; a starch-based gel, soaked in 6 M KOH for 12 h, showed a weight loss of 16% already after 18 h at room temperature (larger times not reported) [80]; a PVA-based gel embedding 1.7 M KOH presented a weight loss of ≈40% after 72 h [81] while a PVA-5 wt.% SiO_2 composite gel, soaked in 6 M KOH for 24 h and exposed to ambient conditions (25ºC, 50% RH), gave a weight loss of 37.6% after 40 h [82]. Sodium polyacrylate (PANa) hydrogel, soaked in 6 M KOH for 24 h and then exposed to air at room temperature, was reported to have only 2.7% weight loss after 185 h [83]; Therefore, embedding the liquid electrolyte in an agarose biopolymer matrix, as shown in this work, greatly retard the time needed for electrolyte evaporation. Compared to other systems found in the literature (60-80% retention, in one case 97%, after few hours), superior electrolyte retention capacity (100-98% retention after 200 h for the gel 8 M KOH) within the agarose biopolymer matrix is here achieved, which also acts as an electrolyte reservoir.

3.2.4. Flexibility tests

The flexibility of the gel based on 8 M KOH embedded in 2 wt.% agarose was determined first visually and then by calculating bending angle using different radii, as shown in **Figure 4**.

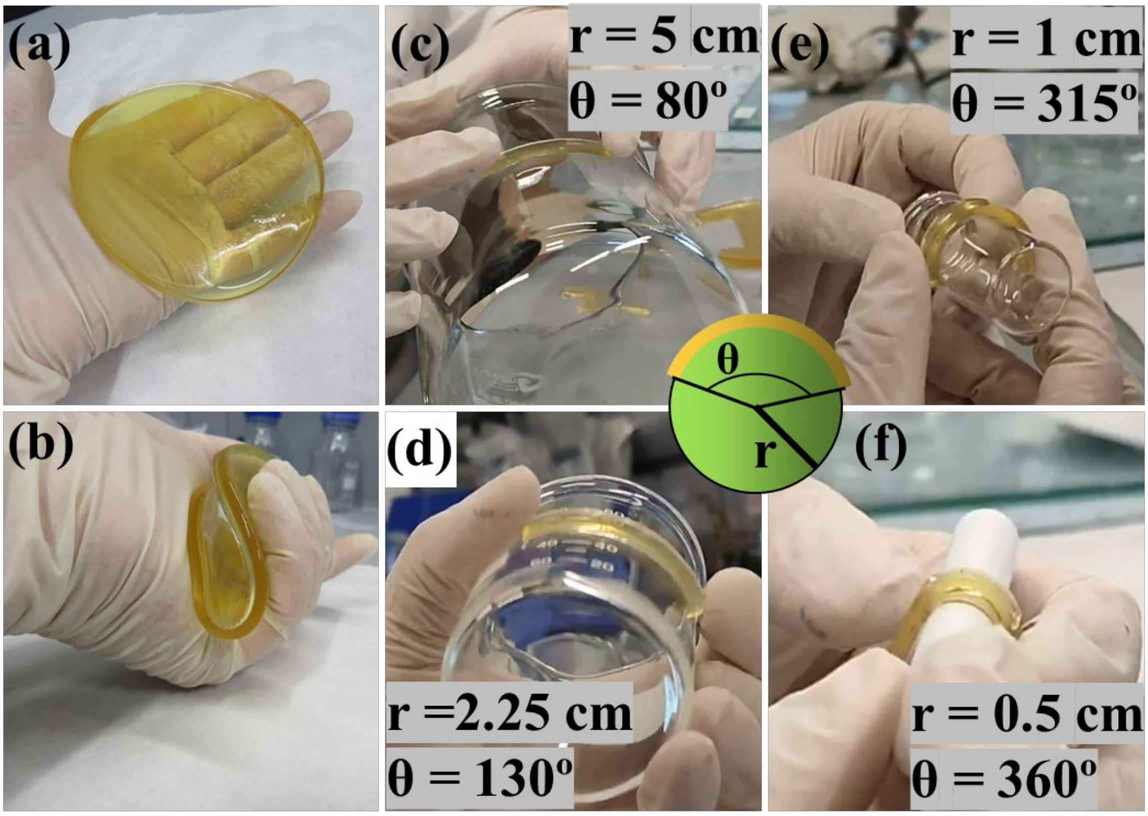

Figure 4. Gel bending test of agarose 2 wt.% biopolymer gel electrolyte with KOH 8 M: (a) not bended; (b) fully bended; (c) 5 cm; (d) 2.25 cm; (e) 1 cm; (f) 0.5 cm (r = radius; θ = arc angle).

The pristine gel seems flexible and mechanically stable and can withstand bending both at small and large angles (**Figure 4a-b**). The experiment was conducted by applying different radii, from big to small radius (5 cm to 0.5 cm, **Figure 4c-f**) at bending, and the measured arc angles (°) are reported in **Figure 4c-f**, together with the radius used. Similar results for the gel 2 wt.% agarose with 6 M KOH (here omitted for brevity, see **Figure S4**) have been achieved.

Overall, the gel shows notable visual flexibility, no water release upon squeezing, and remarkable resistance to repeated bending. Each specimen was deposited onto different circular objects to bend them to different angles, without breaking. The arc angles achieved ranged from 80º to 360º, i.e., completely wrapping the circular support of 0.5 cm radius, the smallest radius tested, considering the size (i.e., 6.5 x 1.0 cm) of the specimen. Usual bending angles reported in the related literature for flexible ZABs are in the range of 0 to 120º, rarely approaching full 180º bending (equivalent to an arc angle of 360º), corresponding to a portion [84] of the arc angles reported in **Figure 4**. The qualitative flexibility test above has shown the possibility to fold the agarose gels up to completely wrapping (i.e., 360º arc angle) a small cylinder, demonstrating the very good flexibility achieved by present agarose-based gels, comparable to already reported synthetic and natural GPEs [69,85,86].

3.2.5. Compression-strain

The ZAB cells used in this work undergo moderate compression when sealed and during battery operation, to ensure component contact. Mechanical testing under uniaxial compression, till failure or cyclically, has been therefore carried out. Compressive strength, ultimate strength, and elastic modulus are determined to compare the elastic behavior of agarose gels 2 wt.% with 6 M or 8 M KOH. The results are shown in **Figure 5**.

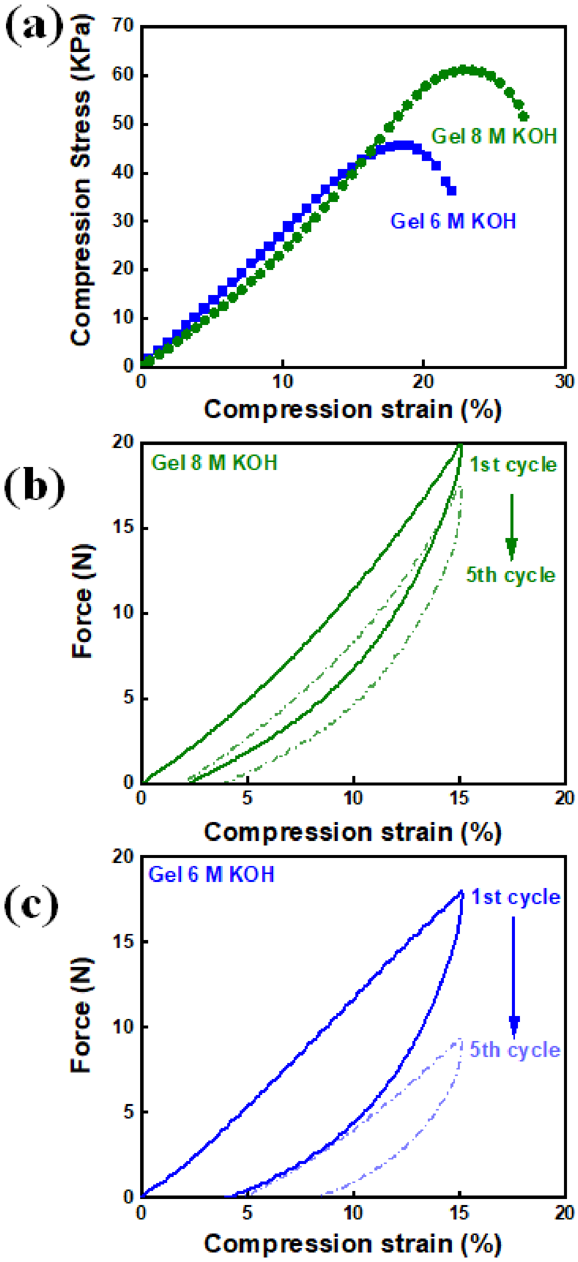

Figure 5. Compression-strain behavior of gels agarose 2 wt.% 6 M and 8 M KOH: (a) failure test under compression; (b) cyclic compression for the 8 M KOH gel; (c) cyclic compression for the 6 M KOH gel.

In **Figure 5a**, the 6 M KOH gel showed approx. linear stress-strain until 16±1% compression strain, followed by the failure of the sample after reaching maximum strain at 22.0±1.0% and maximum stress at 45.0±2.0 kPa. The shape of the curve resembles to what observed in literature for agarose hydrogels prepared in hot water, without any covalent crosslinking [87], and the elastic modulus (at low deformation, 0 to 2% strain) was calculated to be 2.4±0.1 kPa. Differently, the gel 8 M KOH compression tests display a more remarkable progressive compression hardening, eventually leading to sample failure at 27.0±1.0% (green curve in **Figure 5a**). Although the elastic modulus is 2.1±0.2 kPa, very similar to the 6 M KOH gel, the maximum strength was 62.0±1.0 kPa, at 25% compression strain, namely ≈37% higher as compared to 6 M KOH. A brief comparison with the literature is reported in **Table 4**.

Table 4. Comparison of selected mechanical properties for different GPEs.

Gel type	Max compressive strength [MPa]	Strain (at max compression) [%]	Compression modulus [MPa]	Refs.
Agarose 8 M KOH	**$62.0\pm1.0\cdot10^{-3}$**	**25.0±1.0%**	**$2.1\pm0.2\cdot10^{-3}$**	**This work**
Agarose 6 M KOH	**$45.0\pm2.0\cdot10^{-3}$**	**22.0±1.0%**	**$2.4\pm0.1\cdot10^{-3}$**	**This work**
Agarose/LiOH/Urea	0.09-0.33	≈41	-	[87]
Cellulose/NaOH	2.1-7.2	40-50	2-7	[88]
poly(2-acrylamido-2-methylpropanesulfonic acid potassium salt)/methyl cellulose	$170\cdot10^{-3}$	-	-	[89]
PVA/nanocellulose (crosslinked)	$26.2\cdot10^{-3}$	-	-	[90]

shows that Wang et al. [88] reported cellulose/NaOH hydrogels with max. compressive strength in the 2.1-7.2 MPa range (strain 40-50%, compression modulus from 2 to 7 MPa); in another work [87], agarose-based hydrogels showed max. compressive strength from 0.09 to 0.33 MPa (strain up to 41%), while for a poly(2-acrylamido-2-methylpropanesulfonic acid potassium salt)/methyl cellulose gel [89] a max. compressive strength of 170 kPa was reported, and for a borax crosslinked PVA/nanocellulose hydrogel the max. compressive strength was 26.2 kPa [90]. The agarose gels developed in this work show lower compressive strengths because no additional crosslinking or reinforcing additives have been considered in the formulation, to maximize ionic conductivity. Future work will be carried out to also improve the mechanical behavior of these gels.

Cyclic compression tests were conducted to determine the hydrogel properties regarding repeated stress. In these tests, samples were placed between two plates and compressed 5 times up to 15% compression strain to guarantee the sample integrity.

The results reported in **Figure 5b-c** show higher stiffness for 8 M KOH samples compared to 6 M KOH, as higher load is needed to reach 15% deformation, while a lower hysteresis area between compression and decompression plots is observed. In addition to this, the deformation recovery of 6 M KOH sample is lower compared to the 8 M KOH as evidenced by the initial strain shift with increasing the number of compression cycles. The higher stiffness of the gel 8 M KOH with respect to the 6 M KOH might be ascribed to the role of the K^+ cation as the higher concentration in 8 M could lead to a higher propensity of agarose matrix to complex it by hydrogen bonding, while increasing its ionic conductivity.

3.2.6. Preliminary stability study of 8 M KOH gel electrolyte

Finally, a preliminary characterization of gel 8 M KOH stability was carried out in a symmetric cell configuration (i.e., Zn paste/gel biopolymer electrolyte/Zn paste). The evolution of the open circuit voltage (OCV) and internal resistance (IR, taken as the intercept of EIS spectra with the impedance real part axis in the Nyquist plot) are recorded over time. The results are shown in **Figure 6**.

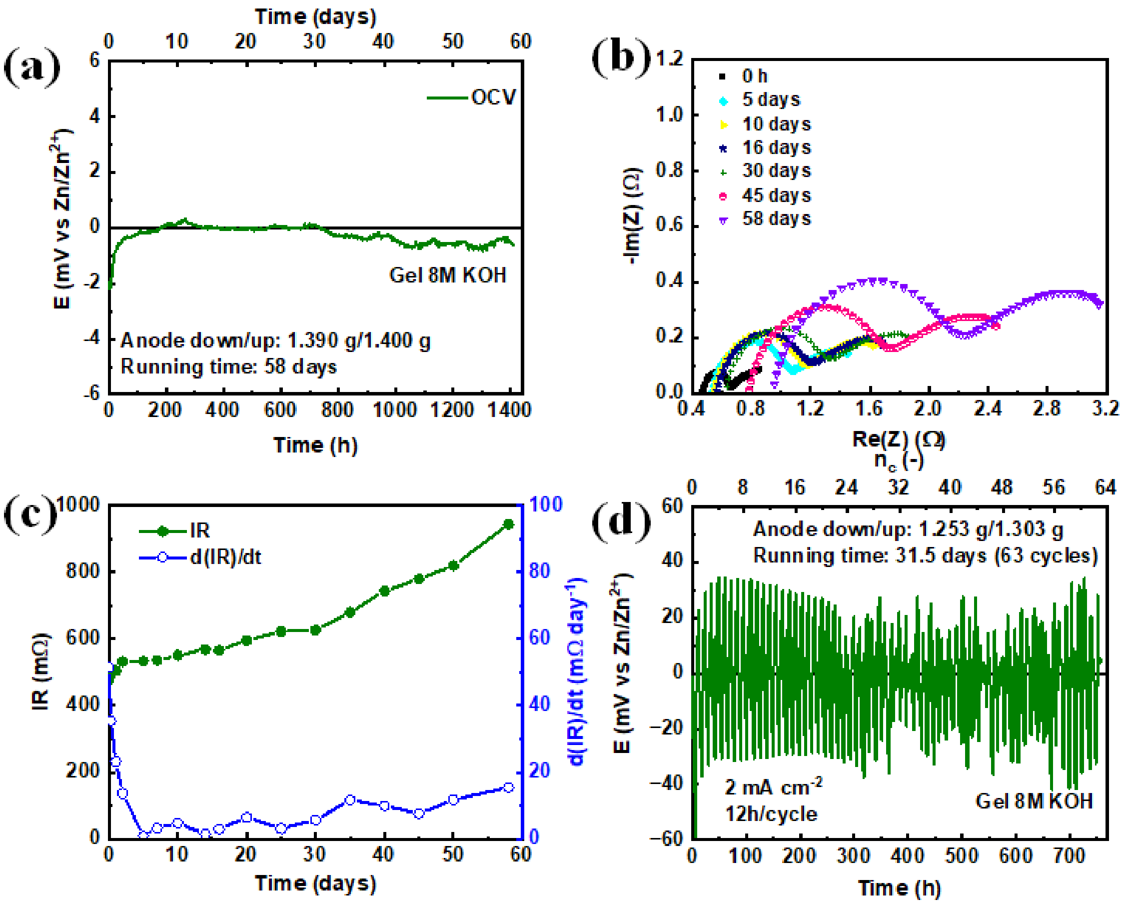

Figure 6. Zn paste/Gel 8 M KOH/Zn paste symmetric cell test of agarose biopolymer gel 8 M KOH: (a) OCV stability over time; (b) EIS spectra evolution; (c) IR evolution; (d) cycling at high areal capacity of 24 mAh cm^{-2}.

In **Figure 6a**, OCV was continuously recorded up to 1400 h (≈58 days), showing an initial stabilization period of approx. 100 h, reaching the equilibrium value of 0 mV as expected. A slight deviation from this value is noticed after 30 days (approx. 700 h) which might indicate the beginning of irreversible Zn corrosion. During the OCV experiment, the impedance response of the symmetric cell was also monitored, and the corresponding EIS spectra, in the frequency range 300 kHz-100 mHz, for selected time points, are shown in **Figure 6b**. Clearly shaped spectra were obtained, evolving with time. At the beginning and up to day 10-16, one close semicircle is visible, reflecting the hindrance of Zn ions and electron movements, as reported by Zhang et al. [91], showing a remarkable ability to maintain a compatible electrode/electrolyte interface under the 10 mV EIS polarization amplitude [92]. From day 30 the tails of EIS spectra, at low frequency, start to exhibit a close shape thus possibly identifying a second semicircle due to a raising second contribution to impedance. Together with the increasing internal resistance and impedance, this could suggest the formation of another interface. We hypothesize that this is due to the formation of a Zn passivation layer due to the prolonged exposition to the alkaline environment. This effect of time on the EIS response of Zn symmetric cells highly depends on the assembly, wettability, and the adhesion between anode and the gel electrolyte [92–94], and would require a dedicated work. The evolution of the IR values is quantified in **Figure 6c**. The assembled symmetric cell presents an initial IR of approx. 500 mΩ that slowly but constantly increases up to approx. 1000 mΩ after 58 days, thus doubling the internal resistance (i.e., the total conductivity is reduced by almost 50%) after 2 months. In **Figure 6c,** the IR increasing rate (i.e., the derivative d(IR)/dt) is also reported. It is observed that after an initial decrease, the rate is <10 mΩ day^{-1} up to 30 days, and then it starts to increase significantly, possibly indicating degradation of the Zn/gel electrolyte interface. In **Figure 6d**, a symmetric cell was cycled at 2 mA cm^{-2} per 12 h/cycle (i.e., 12 mAh cm^{-2}) to explore long cycling conditions at high areal capacity. The results revealed a stable cycling up to approx. 300 h and 24 cycles, and then irregular cycling profile with final failure at approx. 750 h and 63 cycles (total operation 31.5 days). These timing reflects the compatibility and stability observed in **Figure 6a** under OCV and confirms the retard of degradation, mainly ascribed to the corrosion of the Zn paste itself in the high pH environment (**Figure 6b**) rather than to a decomposition of the gel. The overpotential and cycle shape are in line and very similar to those reported in other works [91–93,95] based on gel electrolytes for zinc-ion batteries using Zn metal anodes instead of Zn paste as per this work, demonstrating that the gel itself is suitable for cycling and compatible with zinc. Although encouraging, as said above for EIS, the unique assembly used for the tests, the KOH concentration, and the distribution of the anode, introduce relevant differences with respect to the common standards in the literature, and ad hoc studies of these aspects are needed. This is in accordance with the trend observed for the OCV and the EIS spectra. The result is useful when considering conservation on shelf of assembled cells, with proper protection from air infiltration, to retard degradation. Further work on these aspects is ongoing, and dedicated studies will be done in the future.

3.3. Electrochemical results

3.3.1. Use of gel biopolymer electrolytes in primary ZABs

In primary ZABs, similarly, to the ionic conductivity data discussed in subsection 2.2.2, to choose the optimal concentration of the liquid electrolyte and the solid percentage of the biopolymer, galvanostatic discharges were conducted at 5 mA cm^{-2} varying these parameters. The overall results are shown in **Figure 7**.

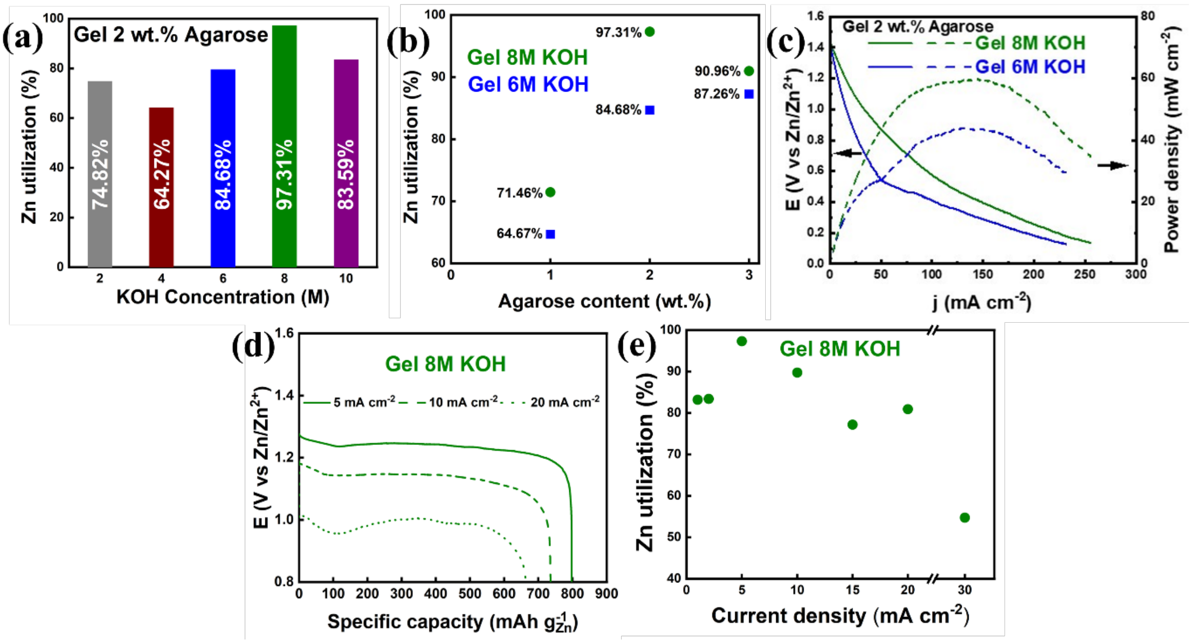

Figure 7. Zn utilization in primary ZABs: (a) 2 wt.% agarose biopolymer gels with different KOH concentrations; (b) gels with 6 M and 8 M KOH at different agarose contents; (c) power density at discharge of gels 6 M and 8M KOH; (d) galvanostatic discharge curves of primary batteries with 8 M KOH (see also **Table 5**) and (e) calculated Zn utilization at different current densities.

In **Figure 7a**, the KOH concentration of the liquid electrolyte embedded in a matrix with 2 wt.% agarose is varied. On average, using the gel 8 M KOH, a zinc extraction of almost 97% can be achieved upon full discharge at 5 mA cm^{-2}. By using 6 M and 10 M KOH gels, interesting Zn utilizations can be achieved, roughly 80% and 84% respectively, that are very close to each other, but far lower than gel 8 M KOH. In **Figure 7b**, 6 M and 8 M KOH liquid electrolytes are used for varying the concentration of the biopolymer within 1 and 3 wt.%. The gels containing 1 wt.% agarose, regardless of the KOH concentration (**Figure 7b**), resulted in low Zn utilization, <72%, while increasing agarose to 3 wt.% sensibly increased the Zn utilization for both 6 M and 8 M KOH from 65 and 72% at 1 wt.% agarose to 87 and 91% at 3 wt.% agarose, respectively. These differences in Zn utilization between gel 8 M and 6 M KOH could be possibly related to factor other than ionic conductivity such as the lower weight losses measured for 8 M gels (**Figure S3**) that might slow down cathode flooding, zinc corrosion and passivation, and the better mechanical behavior that might allow more sealing pressure and better contact within the electrodes. However, the maximum utilization still lays in the gel 2 wt.% agarose 8 M KOH. Moreover, in **Figure 7c**, the polarization curves at discharge and related power densities of full cells assembled with the two gels are shown. The cell with the gel 8 M KOH achieved a maximum power density of 60 mW cm^{-2} whereas the gel 6 M KOH reached 44 mW cm^{-2}, showing also in this case the better performance of the gel 8 M KOH. However, it must be noted that power density strongly depends on cell assembly, geometry, and cathode catalyst employed. Compared to the literature, as reported in [96], ZABs using various GPE and precious cathode catalysts (e.g., Pt, Ir, Co, etc.) have shown power densities in the range 40-140 mW cm^{-2}, hence the result obtained in this work for the gel 8 M KOH is very promising and can be upgraded by using a different cathode. In **Figure 7d**, some representative discharge profiles at increasing current densities are shown. For the selected current densities, all the discharge profiles show a flat plateau, typical of ZABs, and the voltage value of the plateau decreases due to the higher overpotential associated to the higher current densities applied. As a comparison, the discharge profile (5 mA cm^{-2}) of a primary ZAB using a glass fiber separator wetted with a 8 M KOH liquid electrolyte is reported in **Figure S5**, while the discharge profiles using the gel 6 M KOH at different current densities are reported in **Figure S6a**. Finally, **Figure 7e** shows the rate capability of primary ZABs, fully discharged in a large range of current densities (between 1-30 mA cm^{-2}), using the gel 2 wt.% agarose 8 M KOH (for gel with 6 M KOH see **Figure S6b**). The primary ZABs showed a Zn utilization >70% in the 2-15 mA cm^{-2} range for both gels, and notably >80% Zn utilization in the 2-20 mA cm^{-2} range for the gel 8 M

KOH. Moreover, the contact between the gel and the electrodes, before and after discharge, did not show visible compatibility issues upon disassembling and inspection (**Figure S7**). A deeper post-mortem analysis was carried out at the interface between anode and gel to inspect the structure and morphology of discharge products. In **Figure S8**, SEM images of the gel 8 M and 6 M KOH pristine surfaces are compared, showing a very flat and regular surface for the gel 8 M KOH compared with the less regular one of gel 6 M KOH. The surfaces in contact with the Zn anode paste after discharge also show differences in the morphology of the ZnO discharge products where the particles on the 8 M KOH form a uniform veil of regularly shaped short "sticks" whereas for 6 M KOH the sticks appear more irregularly distributed, shaped, and longer. This is further confirmed in **Figure S9**, where the SEM images of the pristine Zn anode paste is compared with the discharged anode in contact with gel 8 M and 6 M KOH. It is clearly visible how the ZnO sticks deposited with the gel 8 M KOH have an average size of approx. 1 μm whereas for the 6 M KOH the size is > 3 μm, probably determining a slower deposition of Zn and formation of bulky irreversible products that could accelerate the growth of crystals and hence the formation of a thick passivation layer hindering capacity extraction. Finally, XRD spectra of Zn paste before and after discharging are shown and discussed in **Figure S10** to determine the chemical nature of the other secondary discharge products formed.

The performance of ZABs with different gel electrolytes are compared within the relevant literature in **Table 5** showing that the results achieved in this work are very notable and that other studies obtained lower ionic conductivity (up to one order of magnitude in some cases) and poorer discharge performance at high rates (> 1-2 mA cm^{-2}). **Table S2** compares our data normalizing discharged capacity by area (anode) for current density values of 2 and 5 mA cm^{-2} (see also **Figure S11**). The discharge capacity by area achieved in this work is almost 600 times higher than that in Zuo et al. [78] at 2 and also 5 mA cm^{-2} specifically using an agar-based gel with a melamine foam.

Table 5. Literature comparison of ionic conductivity and primary discharge performances of GPEs for ZABs with those from this work.

Gel type	Current density [mA cm^{-2}]	Discharge Capacity [mAh g^{-1}]	Zn utilization [%]	Discharge time [min]	Ionic conductivity [S cm^{-1}]	Refs.
Agarose 8 M KOH	5	797.701	97.31	11573	0.451	**This work**
Agarose 8 M KOH	10	735.46	89.72	5024	0.451	**This work**
Agarose 8 M KOH	20	663.12	80.89	2743	0.451	**This work**
Agarose 8 M KOH	30	468.49	57.15	959.00	0.451	**This work**
Agarose 6 M KOH	5	694.12	84.68	9447.42	0.383	**This work**

Agarose 6 M KOH	10	657.62	80.22	4238.59	0.383	**This work**
Agarose 6 M KOH	20	498.95	60.87	1669.50	0.383	**This work**
Agarose 6 M KOH	30	341.09	41.61	790.76	0.383	**This work**
Starch 6 M KOH	2	752.00	91.71	-	0.112	[80]
PVA:PAA (10:7.5) + 32 wt.% KOH	150 mA	1347 mAh	89.80	539	0.300	[97]
PVA/PECH + 32 wt.% KOH	150 mA	1338 mAh	89.00	-	-	[98]
PVA/5wt% SiO$_2$ + 6 M KOH	3	720.60	87.00	-	-	[99]
PAA 6 M KOH	5	684.00	83.44	-	-	[100]
Cellulose + 6 M KOH/Zn acetate	5	695.00	84.00	-	-	[101]
PEO–PVA–glass-fibre-mat + KOH	150 mA	1305 mAh	83.65	522	PEO:PVA (5:5) = 0.048 (7:3) = 0.020	[102]
PVA + 6 M KOH/Zn acetate	5	660.00	80.49	-	-	[103]
hydroponics gel + 6 M KOH	≈4	657.50	80.20	1578	-	[104]
CMC:PAA (1:2) + 8 M KOH	5	641.90	78.84	136	0.231	[51]
PVA + 0.1 M KOH /Zn acetate	5	623.40	76.02	960	-	[105]
PVA + 6 M KOH	2.5 mA cm^{-3}	603.70	73.00	-	-	[106]
PVA + KOH	2	595.00	72.00	>180	-	[107]
PVA + 0.15 KOH	6 mA cm^{-3}	≈550	67.00	-	-	[108]
acrylic acid + K$_2$S$_2$O$_8$, + 4 M KOH	25	530.00	64.63	-	0.288	[109]
Sago + 6 M KOH	100 mA	505.00	61.58	-	0.445	[36]
Nanoporous cellulose + 1 M KOH	25 mA g^{-1}	492.00	60.00	1200	0.0212	[110]
PVA + KOH	250 A L^{-1} [50 A kg $^{-1}$]	460.00	56.00	-	-	[84]
Crosslinked PAA + 11.25 M KOH	25 mA cm^{-3}	>387	>47	-	-	[111]
Agar-PVA/GO + 6 M KOH/ZnCl$_2$	0.5	230.60	28.12	-	0.075	[112]
PVA + 8.3 wt.% KOH	-	-	-	-	0.153	[113]
PVAA-cellulose in 6 M KOH + 0.2 M Zn acetate	3	724.00	88.32	-	0.123	[96]
Liquid 6 M KOH + 0.2 M Zn acetate	10	797.80	97.32	-	-	[114]

Further quantitative information and calculated metrics for the cells in **Figure 7** (i.e., masses, Zn loading, Zn weight fraction, energy density etc.) are fully reported in **Table S3** that can be used for optimization of the single cell, especially for Zn weight fraction and energy density because these two parameters are dependent on the precise assembly, total mass of each component, and mass of active Zn material, that are not always reported in the literature.

The data in **Table 5** are useful for further comparison with literature of reported ionic conductivity, discharged capacity/time, and Zn utilization. For instance, Kwon et al. [100] reported a specific capacity of 684 mAh g^{-1} at 5 mA cm^{-2} using a 6 mol KOH PAA gel; Fu et al. [115] used a porous cellulose film gelled with 6 M KOH and extracted a capacity of 652.6 mAh g^{-1} applying a discharge current of 5 mA cm^{-2}, comparable with the actual agarose gel 6 M KOH while superior values are obtained by the agarose gel 8 M KOH (**Table 5**). Despite the current densities applied were lower, Zuo et al. [80] obtained 752 mAh g^{-1} (at 2 mA cm^{-2}) using a starch/KOH 6 M gel electrolyte, Jiang et al. [116] reported a DMSO-based organo-hydrogel delivering a high specific capacity (700 mAh g^{-1}) always at 2 mA cm^{-2}, while Sun et al. [89] reported a specific capacity of 764.7 mAh·g^{-1} at 1 mA cm^{-2} using a poly(2-acrylamido-2-methylpropanesulfonic acid potassium salt)/methyl cellulose with KOH 6 M. The outstanding overall results obtained for the gel 8 M KOH reported here looks therefore unprecedented (excluding some work with too different assembly and design for comparison) from a wide range of current densities 5-20 mA cm^{-2}.

To further improve results at higher current densities, the mass of Zn could be better distributed by controlling the amount of anode paste, geometry of the anode compartment and thickness to increase discharged capacity, i.e., Zn utilization, and in turn, overall cell energy density. The same applies to the electrolyte because by reducing its thickness as much as possible, without compromising the overall cell operation, Zn weight fraction and energy density could be increased. However, for each current density in **Table 5**, it is demonstrated that the 8 M KOH gel performed better than 6 M KOH, because higher Zn utilization and specific discharged capacity were achieved.

3.3.2. Use of 2 wt.% agarose biopolymer gel electrolyte 8 M KOH in secondary ZABs

The 2 wt.% agarose biopolymer gel with 8 M KOH behaves properly as a solid electrolyte, has excellent electrolyte retention, high ionic conductivity, good flexibility, and robustness. Due to the encouraging performance in primary batteries and the outstanding Zn utilization − unprecedented in the literature −, these results support the possible application of this gel in electrically rechargeable ZABs (ERZAB).

In ERZABs, the validation of cyclability, rechargeability, and performance is complex, and reliable protocols are still under intense debate in the literature [52–54]. Moreover, the debate is centered on the cycling conditions (i.e., current density and cycling time) to be used to test and validate rechargeability. The most frequent approach is to apply mid-to-high current densities (5 or 10 mA cm^{-2}) for very short times (10 or 20 min per cycle) to maximize the number of cycles because parasitic reactions and material degradation experienced by components do not have enough time to occur. On the contrary, low current densities applied for long times (>1-6 h per cycle) could hinder degradation phenomena, due to the low overpotentials, but provide enough time for parasitic reactions to slowly occur after few cycles, hence selecting cycling conditions is not trivial. Recently, to consider industrially relevant applications, the value of 12 mAh cm^{-2} for areal capacity (calculated as the product of current density and discharge time per cycle) was proposed as threshold for ERZABs [54].

Therefore, in this work, at first two current densities and cycling times have been explored as parameters to obtain small areal capacities (i.e., < 12 mAh cm^{-2}) showing their combined effect on number of cycles and calculated performance, and then only current density is varied as parameter with a fixed cycling time of 12 h disc./ch. to obtain larger areal capacities (i.e., ≥ 12 mAh cm^{-2}) to study cyclability and the effect of current density on the number of cycles.

The results of the cyclability tests are shown in **Figure 8**. Furthermore, in **Table S4**, quantitative information and calculated metrics for the ERZAB cells in **Figure 8** (i.e., masses, Zn loading, Zn weight fraction, energy density etc.) are fully reported.

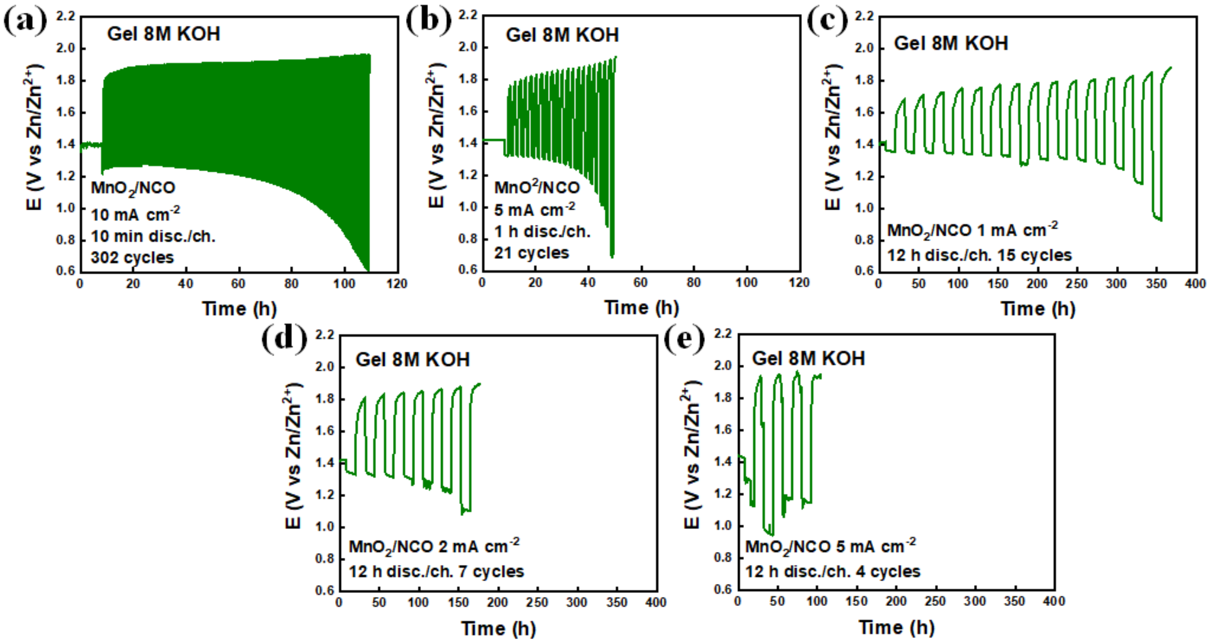

Figure 8. Cyclability tests in ERZAB for short cycles: (a) 10 mA cm^{-2}, 10 min disc./ch. (areal capacity 1.67 mAh cm^{-2}); (b) 5 mA cm^{-2}, 1 h disc./ch. (areal capacity 5 mAh cm^{-2}). Cyclability tests in ERZAB for long cycles: (c) 1 mA cm^{-2} 12 h disc./ch. (areal capacity 12 mAh cm^{-2}); (d) 2 mA cm^{-2}, 12 h disc./ch. (areal capacity 24 mAh cm^{-2}); (e) 5 mA cm^{-2}, 12 h disc./ch. (areal capacity 60 mAh cm^{-2}).

In **Figure 8a**, the cycling conditions used are similar to those frequently reported in the literature (especially for liquid electrolyte). The calculated areal capacity is 1.67 mAh cm^{-2}, showing that the gel 8 M KOH achieved approx. 100 h of continuous operation and 302 cycles, in line with the literature for ERZABs using GPE (see also **Table 7** below). These cycling conditions, alleviating irreversible impacts from the zinc electrode rather than assessing a notable rechargeability [54], are not feasible for practical uses because the areal capacity is far below the indicated threshold, and often quantitative comparisons/calculations are tricky due to missing information about zinc mass and liquid electrolyte in excess [53]. As complementary information, the Voltage *vs.* Specific capacity plots of the cycled cells are reported in **Figure S12** to show in detail the evolution of discharge/charge voltage over cycling as a function of current density and time. It is possible to observe that discharged/charged capacity per cycle are identical, hence providing a Coulombic efficiency of ≈100% (due to the CC cycling mode used) that is retained along operations under all the conditions tested, showing the excellent capacity retention behavior of the developed gel.

To demonstrate the combined and not trivial effect of current density and cycling time, in **Figure 8b** current density was reduced to 5 mA cm^{-2}, while cycling time was increased to 2 h and the calculated areal capacity is 5 mAh cm^{-2}. As a consequence, the operation time and number of cycles drastically decreased to approx. 40 h and 21 cycles. Considering just the number of cycles as parameter to evaluate rechargeability of ERZABs, one would say that the cell achieving 302 cycles is better than the second cell achieving just 21 cycles. This is not correct if one calculates the specific metrics per cycle, together with the round-trip efficiency. This is done for all the cells in **Figure 8** in the following **Table 6**.

Table 6. Secondary cells value per cycle for performance calculation (**Figure 8**, active Zn mass and loading are those reported in **Table S4**).

Current density [mA cm^{-2}]	**Disch./ch. time [h]**	**N. of cycles [-]**	**Disch. capacity per cycle [mAh g$_{Zn}^{-1}$]**	**DoD$_c$ per cycle [%]**	**Energy density per cycle [Wh kg$_{cell}^{-1}$]**	**Disch. voltage, avg. [V]**	**Ch. voltage, avg. [V]**	**Round-trip efficiency [%]**
10	0.167	302	1.25	0.15	0.52	1.11	1.92	57.81
5	1	21	4.40	0.53	1.82	1.20	1.86	64.52
1	12	15	9.30	1.14	4.06	1.25	1.78	70.22
2	12	7	22.50	2.74	9.53	1.25	1.85	67.57
5	12	4	54.80	6.70	20.77	1.12	1.90	58.95

The cell operated at 10 mA cm^{-2} and 0.167 h (areal capacity 1.67 mAh cm^{-2}), gives the highest number of cycles, and therefore the highest cumulative DoD and energy density (see **Table S4**), but presents the lowest metrics per cycle. From **Table 6**, can be concluded that to increase the number of cycles, very short cycle times can be applied, but when longer cycle times are used, the number of cycles decreases but the capacity and energy density per cycle are increased due to the higher areal capacity. This is the reason why large areal capacities are required to meet real applications. Moreover, to obtain a good round-trip efficiency, small current densities must be used to minimize overpotentials, and hence long cycling time are needed to meet the areal capacity threshold of 12 mAh cm^{-2}. Therefore, in **Figure 8c-e**, the cycling time was fixed to a daily cycle (i.e., 24 h per cycle, 12 h discharge and 12 h charge), to test an application-oriented time representing an industrially relevant condition, while current density was varied as parameter from 1 mA cm^{-2} to 2 and 5 mA cm^{-2}. As expected, the areal capacity was progressively increased from 12 to 24 and up to 60 mAh cm^{-2}, while the number of achieved cycles is progressively reduced, indeed almost halved (from 15 to 7 to 4 cycles, respectively at 1, 2, and 5 mA cm^{-2}). These results suggest that the correlation between current density and number of cycles is inversely proportional in these conditions. Cross-comparing **Figure 8b** and **Figure 8e** at the same current density of 5 mA/cm^2 it is demonstrated also that cycle life decreases (from 21 to 4 cycles) when cycling time is increased (from 1 h to 12 h). Therefore, the rate capability of the assembled cells using the gel 8 M KOH is demonstrated by changing both current density and cycling time.

Furthermore, the metrics per cycle under these conditions in **Table 6** are very interesting because, even if the number of achieved cycles is small, the delivered capacity (54.80 mAh g_{Zn}^{-1} per cycle), the energy density (20.77 Wh kg_{cell}^{-1} per cycle), and the round-trip efficiency (58.95%) are higher than the cell operated at 1.67 mAh cm^{-2} for 302 cycles (1.25 mAh g_{Zn}^{-1}, 0.52 Wh kg_{cell}^{-1}, and 57.81%, respectively). This represent a truly industrially relevant result for future scale-up and shows the importance to obtain high areal capacities, while considering only the number of cycles is less relevant for real use.

However, in the profiles of **Figure 8d** and **Figure 8e**, instabilities in discharge voltage, causing deformed cycle shapes and spikes, are visible for many cycles (in **Figure 8c** this randomly occurs only for one discharge cycle). As recently reported in the literature, we ascribe this to the combination of current density and long cycling time, possibly affecting the degradation of cathode during the charge phase [117], the irreversible passivation of zinc-to-zinc oxide, and dendrite formation at gel/anode interface [118]. Moreover, in terms of gel chemical stability under cycling, we observed a change in the color (from yellowish to dark brown) of the electrolyte under any cycling conditions (see **Figure S13**). This is probably due to two phenomena, dissolution of catalyst/carbon support from cathode and/or hydrolysis of gelled liquid electrolyte. During long charges, (e.g., hours) these phenomena are promoted and extended because of the longer time available to occur.

In addition, **Table 6** shows the calculated round-trip efficiency, demonstrating that the cells operated under small areal capacity are not as efficient as the cells operated under higher areal capacity. It is worth noticing that this is more related to the current density applied and overpotentials rather than time and is not directly related to mass and cell assembly/design. However, maximizing the number of cycles is extremely important to improve cyclability and rechargeability, but it should be also obtained at high areal capacity and high round-trip efficiency.

In conclusion, the comparison with the literature in terms of electrode types, electrolyte, cycling conditions (i.e., calculated areal capacity to include both current density and discharge time), the number of cycles, and calculated round trip efficiency is reported in **Table 7**.

Table 7. Comparison of cycling performance in ERZABs with a gel electrolyte.

Gel type	**Anode type**	**Cathode type**	**Areal capacity [mAh cm^{-2}]**	**N. of cycles [-]**	**Round-trip efficiency$^{(a)}$ [%]**	**Refs.**
Agarose 8 M KOH	Zn paste	MnO_2/NCO	1.67	302	57.81	**This work**
Agarose 8 M KOH	Zn paste	MnO_2/NCO	5	21	64.52	**This work**
Agarose 8 M KOH	Zn paste	MnO_2/NCO	12	15	70.22	**This work**
Agarose 8 M KOH	Zn paste	MnO_2/NCO	24	7	67.57	**This work**
Agarose 8 M KOH	Zn paste	MnO_2/NCO	60	4	58.95	**This work**
Agar + melamine foam in 6 M KOH	Zn foil	Mn-Co-Fe@CNT	0.334	74	62.30	[78]
Starch gel saturated with KOH + ZnO	Zn foil	Mn-Co-Fe@CNT	0.167	216	63.54	[80]
PAA 6 M KOH	Electrodeposited Zn	Pt-Ir/C	0.33	100	61.52	[100]
Quaternary ammonium functionalized cellulose in 6 M KOH	Zn foil	S-C_2N aerogel/stainless steel mesh	25	230	63.15	[101]
PAA 6 M KOH	Zn foil	Pt-Ru/C	0.041	25	79.00	[94]

PVA/guar hydroxy propyl trimonium chloride 2 M KOH	Zn foil	IrO_2/Pt/C/carbon cloth	0.167	57	62.12	[119]
BC-PVA in 6 M KOH + 0.2 M Zn acetate	Zn foil	Co_3O_4@Ni foam	0.165	650	69.40	[120]
Crosslinked PVA/PAA in 6 M KOH	Zn powder/PEI/CNT	Co_3O_4@MWCNT	0.041	150	57.69	[121]
PAM crosslinked with MBAa in 6 M KOH	Zn foil	C-CoPAN900/ carbon paper	1 mAh	55	60.91	[122]
PAM/Na-Alginate/KI	Zn foil	PtC/RuO_2	0.167	330	79.14	[123]
PVA + Lecithin in 6 M KOH + 0.2 Zn acetate	Zn foil	CoFeP@C	0.5	141	57.50	[124]
PVAA-cellulose in 6 M KOH + 0.2 M Zn acetate	Zn foil	CoFeP@C	0.5	162	57.60	[96]
Liquid 6 M KOH + 0.2 M $ZnCl_2$	Zn foil	$Mn_{0.5}Ni_{0.5}Co_2O_4$/C	0.7	150	58.58	[125]
Liquid 7 M KOH + ZnO + KF + K_2CO_3	Zn paste	NCO/CNT	2	88	60.00	[126]

(a) Values have been extrapolated from published figures if not explicitly reported in the cited source.

In **Table 7**, ERZABs using a GPE are included together with a couple of examples with liquid electrolytes, and usually the areal capacities calculated are very small, although large numbers of cycles and good round-trip efficiency are reported. Compared to the literature, the ERZABs developed here using the agarose gel with 8 M KOH show a very competitive round-trip efficiency, even at far higher areal capacity than those in the literature, and that the longer cycling times used justify the small number of cycles achieved. This is the aspect to be improved and a better cell and component design could greatly help in achieving more cycles at high areal capacity with the outstanding gel developed in this work. Therefore, data reported above demonstrates that the developed gel 8 M KOH can be used in ERZABs, and can sustain quite well high areal capacities, not previously tested in the relevant literature, although optimizations are needed.

4. Conclusions

The use of naturally occurring biopolymers to synthesize gel electrolytes for ZABs, and batteries in general, is a very appealing approach to replace the use of synthetic polymers, derived from petrochemicals, as alternative to standard liquid electrolytes and related issues.

However, a compromise between physical, chemical, mechanical, and electrochemical properties is needed to design a high-performance gel.

In this work, a more convenient, faster, and scalable synthesis method is proposed to obtain agarose gels directly embedding a highly alkaline and corrosive electrolyte which is applicable also to other biopolymers such as xanthan, agar-agar, and κ-carrageenan, which gave higher ionic conductivity compared to the literature, but still lower than the agarose gel developed within this work. A detailed study of the agarose gels, showing the effect of biopolymer amount and KOH concentration, is provided. Thorough characterization in terms of ionic conductivity, chemical structure, electrolyte retention, flexibility (qualitative) and compression modes (quantitative) is presented, which accounts for the best gel biopolymer electrolyte formulation being the gel with 2wt% agarose and 8 M KOH electrolyte. Indeed, it shows an ionic conductivity of 0.45±0.05 S cm^{-1} at room temperature, elastic modulus is 2.1±0.2 kPa and maximum compression strength of 62.0±1.0 kPa, at 25% of compression strain, with a ≈100% electrolyte retention (i.e., negligible weight loss) up to 200-250 h at 30±1ºC and environmental relative humidity of 40±5%. When this gel was used to for primary ZABs assembly, it provided unprecedented Zn utilization for GPEs in ZABs of ≈97% at 5 mA cm^{-2}, and between 75% and 80% in the 1-20 mA cm^{-2} range, on average.

The biopolymer gel electrolyte was further used in secondary ERZABs and tested under very small (<<12 mAh cm^{-2}) and large (>>12 mAh cm^{-2}) areal capacities to determine the effect of applied current density and cycling time. Promising results were obtained in terms of DoD_c, energy density (total and per cycle), and delivered capacity while satisfying number of cycles were achieved. By using the gel 8 M KOH, >300 cycles were obtained at 10 mA cm^{-2} and 20 min per cycle, but the DoD_c was 0.15% and round-trip efficiency was ≈57%, whereas at 1 mA cm^{-2} and 24 h per cycle, the DoD_c was 1.14%, round-trip efficiency ≈70% on average of 15 cycles. At the hardest cycling conditions tested (5 mA cm^{-2} and 24 h per cycle, corresponding to an areal capacity of 60 mAh cm^{-2}), a DoD_c of 6.7% and a round-trip efficiency of 59% were achieved, with only four reversible cycles achieved. Cyclability results suggested that number of cycles alone is not enough to prove high performance or high round-trip efficiency, as generally reported in the literature, and, as also confirmed by the final EIS characterization on Zn paste/Zn paste symmetric cell, an overall optimization of components, anode mass distribution, cell design, and assembly is needed to better exploit the developed electrolyte and single cells, to increase the number of cycles at high areal capacities and long cycling times. Therefore, the results discussed in this work are a preliminary benchmark to push future research toward a more quantitative, engineered, and integrated approach for component development and performance evaluation by adopting gelled electrolyte and relevant cycling times to assess concrete progress in ZABs and ERZABs.

Supplementary materials information

Supplementary materials are available online or from the authors.

CRediT authorship contribution statement

Conceptualization: N.O.V., E.G.G., M.C.M.M., D.F.; **Methodology:** All authors; **Formal analysis:** E.G.G., D.F., M.C.M.M, L.M.; **Data curation:** E.G.G., D.F.; **Visualization:** E.G.G., D.F. N.O.V; **Investigation:** E.G.G., D.F., M.C.M.M.; **Writing – original draft:** E.G.G:, D.F., L.M. N.O.V; **Writing – review & editing:** All authors; **Supervision:** N.O.V., A.F., C.G.; **Funding acquisition:** N.O.V.

Conflicts of interest

There are no conflicts to declare.

Acknowledgements

E. Garcia thanks the Basque Government for the Bikaintek grant (1-AF-W2-2019-00003) N. Ortiz-Vitoriano acknowledges the “Ramón y Cajal” grant (RYC2020-030104-I / AEI / 10.13039/501100011033). Authors are also very thankful to Ainhoa Bustinza Murguialday for her technical support during the experimental trials.

References

[1] J. Zhou, J. Cheng, B. Wang, H. Peng, J. Lu, Flexible metal–gas batteries: a potential option for next-generation power accessories for wearable electronics, Energy Environ Sci. 13 (2020) 1933–1970. https://doi.org/10.1039/D0EE00039F.

[2] X. Chen, Z. Zhou, H.E. Karahan, Q. Shao, L. Wei, Y. Chen, Recent Advances in Materials and Design of Electrochemically Rechargeable Zinc–Air Batteries, Small. 14 (2018) 1801929. https://doi.org/10.1002/smll.201801929.

[3] F. Santos, A. Urbina, J. Abad, R. López, C. Toledo, A.J. Fernández Romero, Environmental and economical assessment for a sustainable Zn/air battery, Chemosphere. 250 (2020) 126273. https://doi.org/10.1016/j.chemosphere.2020.126273.

[4] D. Ahuja, V. Kalpna, P.K. Varshney, Metal air battery: A sustainable and low cost material for energy storage, J Phys Conf Ser. 1913 (2021) 012065. https://doi.org/10.1088/1742-6596/1913/1/012065.

[5] Y. Xu, X. Xu, M. Guo, G. Zhang, Y. Wang, Research Progresses and Challenges of Flexible Zinc Battery, Front Chem. 10 (2022). https://doi.org/10.3389/fchem.2022.827563.

[6] P. Gu, M. Zheng, Q. Zhao, X. Xiao, H. Xue, H. Pang, Rechargeable zinc–air batteries: a promising way to green energy, J Mater Chem A Mater. 5 (2017) 7651–7666. https://doi.org/10.1039/C7TA01693J.

[7] M. Xu, D.G. Ivey, Z. Xie, W. Qu, Rechargeable Zn-air batteries: Progress in electrolyte development and cell configuration advancement, J Power Sources. 283 (2015) 358–371. https://doi.org/10.1016/j.jpowsour.2015.02.114.

[8] L. Jörissen, Secondary aqueous zinc-air battery—Electrically rechargeable, in: Electrochemical Power Sources: Fundamentals, Systems, and Applications, Elsevier, 2021: pp. 81–97. https://doi.org/10.1016/B978-0-444-64333-9.00005-9.

[9] X. Liu, X. Fan, B. Liu, J. Ding, Y. Deng, X. Han, C. Zhong, W. Hu, Mapping the Design of Electrolyte Materials for Electrically Rechargeable Zinc–Air Batteries, Advanced Materials. 33 (2021) 2006461. https://doi.org/10.1002/adma.202006461.

[10] S. Hosseini, S. Masoudi Soltani, Y.-Y. Li, Current status and technical challenges of electrolytes in zinc–air batteries: An in-depth review, Chemical Engineering Journal. 408 (2021) 127241. https://doi.org/10.1016/j.cej.2020.127241.

[11] M.T. Tsehaye, F. Alloin, C. Iojoiu, R.A. Tufa, D. Aili, P. Fischer, S. Velizarov, Membranes for zinc-air batteries: Recent progress, challenges and perspectives, J Power Sources. 475 (2020) 228689. https://doi.org/10.1016/j.jpowsour.2020.228689.

[12] K. Lu, T. Jiang, H. Hu, M. Wu, Hydrogel Electrolytes for Quasi-Solid Zinc-Based Batteries, Front Chem. 8 (2020). https://doi.org/10.3389/fchem.2020.546728.

[13] J. Lu, P. Jaumaux, T. Wang, C. Wang, G. Wang, Recent progress in quasi-solid and solid polymer electrolytes for multivalent metal-ion batteries, J Mater Chem A Mater. 9 (2021) 24175–24194. https://doi.org/10.1039/D1TA06606D.

[14] P. Zhang, K. Wang, P. Pei, Y. Zuo, M. Wei, X. Liu, Y. Xiao, J. Xiong, Selection of hydrogel electrolytes for flexible zinc–air batteries, Mater Today Chem. 21 (2021) 100538. https://doi.org/10.1016/j.mtchem.2021.100538.

[15] S. Lorca, F. Santos, A.J. Fernández Romero, A Review of the Use of GPEs in Zinc-Based Batteries. A Step Closer to Wearable Electronic Gadgets and Smart Textiles, Polymers (Basel). 12 (2020) 2812. https://doi.org/10.3390/polym12122812.

[16] C. Xia, Y. Zhou, C. He, A.I. Douka, W. Guo, K. Qi, B.Y. Xia, Recent Advances on Electrospun Nanomaterials for Zinc–Air Batteries, Small Science. 1 (2021) 2100010. https://doi.org/10.1002/smsc.202100010.

[17] M. Yin, H. Miao, J. Dang, B. Chen, J. Zou, G. Chen, H. Li, High-performance alkaline hybrid zinc batteries with heterostructure nickel/cobalt sulfide, J Power Sources. 545 (2022) 231902. https://doi.org/10.1016/j.jpowsour.2022.231902.

[18] B. Chen, H. Miao, M. Yin, R. Hu, L. Xia, C. Zhang, J. Yuan, Mn-based spinels evolved from layered manganese dioxides at mild temperature for the robust flexible quasi-solid-state zinc-air batteries, Chemical Engineering Journal. 417 (2021) 129179. https://doi.org/10.1016/j.cej.2021.129179.

[19] D. Bresser, D. Buchholz, A. Moretti, A. Varzi, S. Passerini, Alternative binders for sustainable electrochemical energy storage – the transition to aqueous electrode processing and bio-derived polymers, Energy Environ Sci. 11 (2018) 3096–3127. https://doi.org/10.1039/C8EE00640G.

[20] X. Fu, W. Zhong, Biomaterials for High-Energy Lithium-Based Batteries: Strategies, Challenges, and Perspectives, Adv Energy Mater. 9 (2019) 1901774. https://doi.org/10.1002/aenm.201901774.

[21] M.F. Bósquez-Cáceres, S. Hidalgo-Bonilla, V. Morera Córdova, R.M. Michell, J.P. Tafur, Nanocomposite Polymer Electrolytes for Zinc and Magnesium Batteries: From Synthetic to Biopolymers, Polymers (Basel). 13 (2021) 4284. https://doi.org/10.3390/polym13244284.

[22] R. Singh, H.-W. Rhee, The rise of bio-inspired energy devices, Energy Storage Mater. 23 (2019) 390–408. https://doi.org/10.1016/j.ensm.2019.04.030.

[23] P.K. Varshney, S. Gupta, Natural polymer-based electrolytes for electrochemical devices: a review, Ionics (Kiel). 17 (2011) 479–483. https://doi.org/10.1007/s11581-011-0563-1.

[24] A.B. Balaji, H. Pakalapati, M. Khalid, R. Walvekar, H. Siddiqui, Natural and synthetic biocompatible and biodegradable polymers, in: Biodegradable and Biocompatible Polymer Composites, Elsevier, 2018: pp. 3–32. https://doi.org/10.1016/B978-0-08-100970-3.00001-8.

[25] E. Lizundia, D. Kundu, Advances in Natural Biopolymer-Based Electrolytes and Separators for Battery Applications, Adv Funct Mater. 31 (2021) 2005646. https://doi.org/10.1002/adfm.202005646.

[26] C. Wang, T. Yokota, T. Someya, Natural Biopolymer-Based Biocompatible Conductors for Stretchable Bioelectronics, Chem Rev. 121 (2021) 2109–2146. https://doi.org/10.1021/acs.chemrev.0c00897.

[27] M. Gallo, G. Arrighi, L. Moreschi, A. Del Borghi, A. Athanassiou, G. Perotto, Life Cycle Assessment of a Circular Economy Process for Tray Production via Water-Based Upcycling of Vegetable Waste, ACS Sustain Chem Eng. 10 (2022) 13936–13944. https://doi.org/10.1021/acssuschemeng.2c02942.

[28] M.R. Yates, C.Y. Barlow, Life cycle assessments of biodegradable, commercial biopolymers—A critical review, Resour Conserv Recycl. 78 (2013) 54–66. https://doi.org/10.1016/j.resconrec.2013.06.010.

[29] M. Ayala, M. Thomsen, M. Pizzol, Life Cycle Assessment of pilot scale production of seaweed-based bioplastic, Algal Res. 71 (2023) 103036. https://doi.org/10.1016/j.algal.2023.103036.

[30] N. Nanda, N. Bharadvaja, Algal bioplastics: current market trends and technical aspects, Clean Technol Environ Policy. 24 (2022) 2659–2679. https://doi.org/10.1007/s10098-022-02353-7.

[31] K. Alba, V. Kontogiorgos, Seaweed Polysaccharides (Agar, Alginate Carrageenan), in: Encyclopedia of Food Chemistry, Elsevier, 2019: pp. 240–250. https://doi.org/10.1016/B978-0-08-100596-5.21587-4.

[32] M. Osinska-Broniarz, A. Martyla, R. Manczak, A. Sierczynska, Agar as a compound of alkaline solid polymer electrolyte, WSEAS Transactions on Environment and Development. 14 (2018) 474–480.

[33] S.Y. Liew, J.C. Juan, C.W. Lai, G.-T. Pan, T.C.-K. Yang, T.K. Lee, An eco-friendly water-soluble graphene-incorporated agar gel electrolyte for magnesium-air batteries, Ionics (Kiel). 25 (2019) 1291–1301. https://doi.org/10.1007/s11581-018-2710-4.

[34] P.M. Spaziante, A. Nidola, Rechargeable zinc halogen battery, US4181777A, 1980.

[35] E. Raphael, C.O. Avellaneda, M.A. Aegerter, M.M. Silva, A. Pawlicka, Agar-Based Gel Electrolyte for Electrochromic Device Application, Molecular Crystals and Liquid Crystals. 554 (2012) 264–272. https://doi.org/10.1080/15421406.2012.634349.

[36] M.N. Masri, M.F.M. Nazeri, A.A. Mohamad, Sago Gel Polymer Electrolyte for Zinc-Air Battery, in: 5th FORUM ON NEW MATERIALS PART A, Trans Tech Publications Ltd, 2010: pp. 305–308. https://doi.org/10.4028/www.scientific.net/AST.72.305.

[37] R. Othman, A.H. Yahaya, A.K. Arof, A zinc–air cell employing a porous zinc electrode fabricated from zinc–graphite-natural biodegradable polymer paste, J Appl Electrochem. 32 (2002) 1347–1353. https://doi.org/10.1023/A:1022619414787.

[38] J. Menzel, E. Frąckowiak, K. Fic, Agar-based aqueous electrolytes for electrochemical capacitors with reduced self-discharge, Electrochim Acta. 332 (2020) 135435. https://doi.org/10.1016/j.electacta.2019.135435.

[39] L. An, T.S. Zhao, L. Zeng, Agar chemical hydrogel electrode binder for fuel-electrolyte-fed fuel cells, Appl Energy. 109 (2013) 67–71. https://doi.org/10.1016/j.apenergy.2013.03.077.

[40] W.G. Moon, G.-P. Kim, M. Lee, H.D. Song, J. Yi, A Biodegradable Gel Electrolyte for Use in High-Performance Flexible Supercapacitors, ACS Appl Mater Interfaces. 7 (2015) 3503–3511. https://doi.org/10.1021/am5070987.

[41] H. Ueno, Y. Endo, Y. Kaburagi, M. Kaneko, New ionically conductive solids of polysaccharides containing excess water, Journal of Electroanalytical Chemistry. 570 (2004) 95–100. https://doi.org/10.1016/j.jelechem.2004.02.031.

[42] F. Liu, J. Liu, Agarose Based Solid Electrolyte for All-Solid-State Lithium Ion Batteries Working from −20 °C to 80 °C, J Electrochem Soc. 167 (2020) 080519. https://doi.org/10.1149/1945-7111/ab8925.

[43] P. Sun, J. Chen, Y. Huang, J.-H. Tian, S. Li, G. Wang, Q. Zhang, Z. Tian, L. Zhang, High-Strength agarose gel electrolyte enables long-endurance wearable Al-air batteries with greatly suppressed self-corrosion, Energy Storage Mater. 34 (2021) 427–435. https://doi.org/10.1016/j.ensm.2020.10.009.

[44] T. Lin, M. Shi, F. Huang, J. Peng, Q. Bai, J. Li, M. Zhai, One-Pot Synthesis of a Double-Network Hydrogel Electrolyte with Extraordinarily Excellent Mechanical Properties for a Highly Compressible and Bendable Flexible Supercapacitor, ACS Appl Mater Interfaces. 10 (2018) 29684–29693. https://doi.org/10.1021/acsami.8b11377.

[45] P. Sun, W. Liu, D. Yang, Y. Zhang, W. Xiong, S. Li, J. Chen, J. Tian, L. Zhang, Stable Zn anodes enabled by high-modulus agarose gel electrolyte with confined water molecule mobility, Electrochim Acta. 429 (2022) 140985. https://doi.org/10.1016/j.electacta.2022.140985.

[46] M.N. Masri, A.A. Mohamad, Effect of adding potassium hydroxide to an agar binder for use as the anode in Zn–air batteries, Corros Sci. 51 (2009) 3025–3029. https://doi.org/10.1016/j.corsci.2009.08.027.

[47] S. Han, X. Hu, J. Wang, X. Fang, Y. Zhu, Novel Route to Fe-Based Cathode as an Efficient Bifunctional Catalysts for Rechargeable Zn-Air Battery, Adv Energy Mater. 8 (2018) 1800955. https://doi.org/10.1002/aenm.201800955.

[48] Y. Zhang, M. Zhao, Q. Yang, M. Lai, J. Zhang, C. Liu, X. Xu, J. Jia, Agarose-gel-based self-limiting synthesis of a bimetal (Fe and Co)-doped composite as a bifunctional catalyst for a zinc-air battery, J Colloid Interface Sci. 635 (2023) 186–196. https://doi.org/10.1016/j.jcis.2022.12.138.

[49] V. Jose, J.M.V. Nsanzimana, H. Hu, J. Choi, X. Wang, J. Lee, Highly Efficient Oxygen Reduction Reaction Activity of N-Doped Carbon–Cobalt Boride Heterointerfaces, Adv Energy Mater. 11 (2021) 2100157. https://doi.org/10.1002/aenm.202100157.

[50] G.-P. Kim, H.-H. Sun, A. Manthiram, Design of a sectionalized MnO2-Co3O4 electrode via selective electrodeposition of metal ions in hydrogel for enhanced electrocatalytic activity in metal-air batteries, Nano Energy. 30 (2016) 130–137. https://doi.org/10.1016/j.nanoen.2016.10.003.

[51] E. García-Gaitán, D. Frattini, I. Ruiz de Larramendi, M. Martínez-Ibáñez, D. González, M. Armand, N. Ortiz-Vitoriano, Flexible Gel Polymer Electrolytes Based on Carboxymethyl Cellulose Blended with Polyvinyl Alcohol or Polyacrylic Acid for Zinc-Air Batteries, Batter Supercaps. (2023). https://doi.org/10.1002/batt.202200570.

[52] B.J. Hopkins, C.N. Chervin, J.F. Parker, J.W. Long, D.R. Rolison, An Areal-Energy Standard to Validate Air-Breathing Electrodes for Rechargeable Zinc–Air Batteries, Adv Energy Mater. 10 (2020) 2001287. https://doi.org/10.1002/aenm.202001287.

[53] D. Frattini, E. García-Gaitán, A. Bustinza Murguialday, M. Armand, N. Ortiz Vitoriano, Essential data for industrially relevant development of bifunctional cathodes

and biopolymer electrolytes in solid-state Zinc-air secondary batteries, Energy Environ Sci. (2022). https://doi.org/10.1039/D2EE02421G.

[54] J.F. Parker, J.S. Ko, D.R. Rolison, J.W. Long, Translating Materials-Level Performance into Device-Relevant Metrics for Zinc-Based Batteries, Joule. 2 (2018) 2519–2527. https://doi.org/10.1016/j.joule.2018.11.007.

[55] J.-Y. Xiong, J. Narayanan, X.-Y. Liu, T.K. Chong, S.B. Chen, T.-S. Chung, Topology Evolution and Gelation Mechanism of Agarose Gel, J Phys Chem B. 109 (2005) 5638–5643. https://doi.org/10.1021/jp044473u.

[56] M. Tako, S. Nakamura, Gelation mechanism of agarose, Carbohydr Res. 180 (1988) 277–284. https://doi.org/10.1016/0008-6215(88)80084-3.

[57] M. Rinaudo, Seaweed Polysaccharides, in: Comprehensive Glycoscience, Elsevier, 2007: pp. 691–735. https://doi.org/10.1016/B978-044451967-2/00140-9.

[58] S. Yarnpakdee, S. Benjakul, P. Kingwascharapong, Physico-chemical and gel properties of agar from Gracilaria tenuistipitata from the lake of Songkhla, Thailand, Food Hydrocoll. 51 (2015) 217–226. https://doi.org/10.1016/j.foodhyd.2015.05.004.

[59] S. Kondaveeti, K. Prasad, A.K. Siddhanta, Functional modification of agarose: A facile synthesis of a fluorescent agarose-tryptophan based hydrogel, Carbohydr Polym. 97 (2013) 165–171. https://doi.org/10.1016/j.carbpol.2013.04.034.

[60] G.K. Mehta, S. Kondaveeti, A.K. Siddhanta, Facile synthesis of agarose-l-phenylalanine ester hydrogels, Polym Chem. 2 (2011) 2334. https://doi.org/10.1039/c1py00250c.

[61] T.J. Trivedi, D. Bhattacharjya, J.-S. Yu, A. Kumar, Functionalized Agarose Self-Healing Ionogels Suitable for Supercapacitors, ChemSusChem. 8 (2015) 3294–3303. https://doi.org/10.1002/cssc.201500648.

[62] M. Kačuráková, M. Mathlouthi, FTIR and laser-Raman spectra of oligosaccharides in water: characterization of the glycosidic bond, Carbohydr Res. 284 (1996) 145–157. https://doi.org/10.1016/0008-6215(95)00412-2.

[63] Y. Katayama, T. Okanishi, H. Muroyama, T. Matsui, K. Eguchi, Enhanced Supply of Hydroxyl Species in CeO $_2$ -Modified Platinum Catalyst Studied by in Situ ATR-FTIR Spectroscopy, ACS Catal. 6 (2016) 2026–2034. https://doi.org/10.1021/acscatal.6b00108.

[64] M. Ludvigsson, J. Lindgren, J. Tegenfeldt, FTIR study of water in cast Nafion films, Electrochim Acta. 45 (2000) 2267–2271. https://doi.org/10.1016/S0013-4686(99)00438-7.

[65] Z.H. Ping, Q.T. Nguyen, S.M. Chen, J.Q. Zhou, Y.D. Ding, States of water in different hydrophilic polymers — DSC and FTIR studies, Polymer (Guildf). 42 (2001) 8461–8467. https://doi.org/10.1016/S0032-3861(01)00358-5.

[66] R. Gilliam, J. Graydon, D. Kirk, S. Thorpe, A review of specific conductivities of potassium hydroxide solutions for various concentrations and temperatures, Int J Hydrogen Energy. 32 (2007) 359–364. https://doi.org/10.1016/j.ijhydene.2006.10.062.

[67] Y.N. Sudhakar, M. Selvakumar, D.K. Bhat, An introduction of Biopolymer Electrolytes, 2018. https://doi.org/10.1016/b978-0-12-813447-4.00001-7.

[68] M.N. Hafiza, M.I.N. Isa, Conduction mechanism via correlated barrier hopping in EC-plasticized 2-hydroxyehyl cellulose-ammonium nitrate solid polymer electrolyte, IOP Conf Ser Mater Sci Eng. 440 (2018) 012039. https://doi.org/10.1088/1757-899X/440/1/012039.

[69] J. Zhang, J. Fu, X. Song, G. Jiang, H. Zarrin, P. Xu, K. Li, A. Yu, Z. Chen, Laminated Cross-Linked Nanocellulose/Graphene Oxide Electrolyte for Flexible Rechargeable Zinc-Air Batteries, Adv Energy Mater. 6 (2016) 1600476. https://doi.org/10.1002/aenm.201600476.

[70] M.F. Shukur, Y.M. Yusof, S.M.M. Zawawi, H.A. Illias, M.F.Z. Kadir, Conductivity and transport studies of plasticized chitosan-based proton conducting biopolymer electrolytes, Phys Scr. T157 (2013) 014050. https://doi.org/10.1088/0031-8949/2013/T157/014050.

[71] S. Rudhziah, N.A.C. Apandi, R.H.Y. Subban, N.S. Mohamed, Ionic Conductivity of Biopolymer Electrolytes Based on Seaweed kappa-carrageenan, Science Letters. 12 (2018) 45–52.

[72] A. Lewandowski, K. Skorupska, J. Malinska, Novel poly(vinyl alcohol)-KOH-H2O alkaline polymer electrolyte, Solid State Ion. 133 (2000) 265–271. https://doi.org/10.1016/S0167-2738(00)00733-5.

[73] A. Mohamad, N.S. Mohamed, M.Z.A. Yahya, R. Othman, S. Ramesh, Y. Alias, A.K. Arof, Ionic conductivity studies of poly(vinyl alcohol) alkaline solid polymer electrolyte and its use in nickel–zinc cells, Solid State Ion. 156 (2003) 171–177. https://doi.org/10.1016/S0167-2738(02)00617-3.

[74] F. Santos, J.P. Tafur, J. Abad, A.J. Fernández Romero, Structural modifications and ionic transport of PVA-KOH hydrogels applied in Zn/Air batteries, Journal of Electroanalytical Chemistry. 850 (2019) 113380. https://doi.org/10.1016/j.jelechem.2019.113380.

[75] C.-C. Yang, S.-J. Lin, G.-M. Wu, Study of ionic transport properties of alkaline poly(vinyl) alcohol-based polymer electrolytes, Mater Chem Phys. 92 (2005) 251–255. https://doi.org/10.1016/j.matchemphys.2005.01.022.

[76] C.-C. Yang, Chemical composition and XRD analyses for alkaline composite PVA polymer electrolyte, Mater Lett. 58 (2004) 33–38. https://doi.org/10.1016/S0167-577X(03)00409-9.

[77] Y. Yang, T. Wang, Y. Guo, P. Liu, X. Han, D. Wu, Agar-PVA/GO double network gel electrolyte for high performance flexible zinc-air batteries, Mater Today Chem. 29 (2023) 101384. https://doi.org/10.1016/j.mtchem.2023.101384.

[78] Y. Zuo, K. Wang, M. Wei, P. Zhang, S. Zhao, P. Pei, H. Wang, Z. Chen, N. Shang, An Agar gel modulation with melamine foam skeleton for flexible Zn-air batteries, Chemical Engineering Journal. 452 (2023) 139301. https://doi.org/10.1016/j.cej.2022.139301.

[79] Q. Liu, R. Liu, C. He, C. Xia, W. Guo, Z.-L. Xu, B.Y. Xia, Advanced polymer-based electrolytes in zinc–air batteries, EScience. 2 (2022) 453–466. https://doi.org/10.1016/j.esci.2022.08.004.

[80] Y. Zuo, K. Wang, M. Wei, S. Zhao, P. Zhang, P. Pei, Starch gel for flexible rechargeable zinc-air batteries, Cell Rep Phys Sci. 3 (2022) 100687. https://doi.org/10.1016/j.xcrp.2021.100687.

[81] Y. Li, X. Fan, X. Liu, S. Qu, J. Liu, J. Ding, X. Han, Y. Deng, W. Hu, C. Zhong, Long-battery-life flexible zinc–air battery with near-neutral polymer electrolyte and nanoporous integrated air electrode, J Mater Chem A Mater. 7 (2019) 25449–25457. https://doi.org/10.1039/C9TA09137H.

[82] X. Fan, J. Liu, Z. Song, X. Han, Y. Deng, C. Zhong, W. Hu, Porous nanocomposite gel polymer electrolyte with high ionic conductivity and superior electrolyte retention capability for long-cycle-life flexible zinc–air batteries, Nano Energy. 56 (2019) 454–462. https://doi.org/10.1016/j.nanoen.2018.11.057.

[83] Y. Huang, Z. Li, Z. Pei, Z. Liu, H. Li, M. Zhu, J. Fan, Q. Dai, M. Zhang, L. Dai, C. Zhi, Solid-State Rechargeable Zn//NiCo and Zn-Air Batteries with Ultralong Lifetime and High Capacity: The Role of a Sodium Polyacrylate Hydrogel Electrolyte, Adv Energy Mater. 8 (2018) 1802288. https://doi.org/10.1002/aenm.201802288.

[84] J. Fu, D.U. Lee, F.M. Hassan, L. Yang, Z. Bai, M.G. Park, Z. Chen, Flexible High-Energy Polymer-Electrolyte-Based Rechargeable Zinc-Air Batteries, Advanced Materials. 27 (2015) 5617–5622. https://doi.org/10.1002/adma.201502853.

[85] L. Ma, S. Chen, D. Wang, Q. Yang, F. Mo, G. Liang, N. Li, H. Zhang, J.A. Zapien, C. Zhi, Super-Stretchable Zinc–Air Batteries Based on an Alkaline-Tolerant Dual-Network Hydrogel Electrolyte, Adv Energy Mater. 9 (2019) 1803046. https://doi.org/10.1002/aenm.201803046.

[86] Z. Wang, H. Li, Z. Tang, Z. Liu, Z. Ruan, L. Ma, Q. Yang, D. Wang, C. Zhi, Hydrogel Electrolytes for Flexible Aqueous Energy Storage Devices, Adv Funct Mater. 28 (2018) 1804560. https://doi.org/10.1002/adfm.201804560.

[87] S. Wang, R. Zhang, Y. Yang, S. Wu, Y. Cao, A. Lu, L. Zhang, Strength enhanced hydrogels constructed from agarose in alkali/urea aqueous solution and their application, Chemical Engineering Journal. 331 (2018) 177–184. https://doi.org/10.1016/j.cej.2017.08.118.

[88] H. Wang, J. Wu, J. Qiu, K. Zhang, J. Shao, L. Yan, *In situ* formation of a renewable cellulose hydrogel electrolyte for high-performance flexible all-solid-state asymmetric supercapacitors, Sustain Energy Fuels. 3 (2019) 3109–3115. https://doi.org/10.1039/C9SE00339H.

[89] N. Sun, F. Lu, Y. Yu, L. Su, X. Gao, L. Zheng, Alkaline Double-Network Hydrogels with High Conductivities, Superior Mechanical Performances, and Antifreezing Properties for Solid-State Zinc–Air Batteries, ACS Appl Mater Interfaces. 12 (2020) 11778–11788. https://doi.org/10.1021/acsami.0c00325.

[90] M. Chen, J. Chen, W. Zhou, J. Xu, C.-P. Wong, High-performance flexible and self-healable quasi-solid-state zinc-ion hybrid supercapacitor based on borax-crosslinked polyvinyl alcohol/nanocellulose hydrogel electrolyte, J Mater Chem A Mater. 7 (2019) 26524–26532. https://doi.org/10.1039/C9TA10944G.

[91] D. Zhang‡, H. Lu‡, N. Lyu‡, X. Jiang, Z. Zhang, Y. Jin, 200 MPa cold isostatic pressing creates surface-microcracks in a Zn foil for scalable and long-life zinc anodes, Nanoscale Adv. 5 (2023) 934–942. https://doi.org/10.1039/D2NA00682K.

[92] B. Zhang, L. Qin, Y. Fang, Y. Chai, X. Xie, B. Lu, S. Liang, J. Zhou, Tuning Zn2+ coordination tunnel by hierarchical gel electrolyte for dendrite-free zinc anode, Sci Bull (Beijing). 67 (2022) 955–962. https://doi.org/10.1016/j.scib.2022.01.027.

[93] S. Chen, P. Sun, J. Humphreys, P. Zou, M. Zhang, G. Jeerh, S. Tao, Acetate-based 'oversaturated gel electrolyte' enabling highly stable aqueous Zn-MnO2 battery, Energy Storage Mater. 42 (2021) 240–251. https://doi.org/10.1016/j.ensm.2021.07.033.

[94] T.N.T. Tran, H.-J. Chung, D.G. Ivey, A study of alkaline gel polymer electrolytes for rechargeable zinc–air batteries, Electrochim Acta. 327 (2019) 135021. https://doi.org/10.1016/j.electacta.2019.135021.

[95] C. Xi, Y. Xiao, C. Yang, M. Li, L. Li, Y. Chao, L. Li, C. He, Y. Yu, Localized gelation cellulose separators enable dendrite-free anodes for future zinc-ion batteries, J Mater Chem A Mater. 11 (2023) 6522–6529. https://doi.org/10.1039/D3TA00094J.

[96] W. Li, Y. Wang, R. Liu, W. Chen, H. Zhang, Z. Zhang, Gel Polymer-Based Composite Solid-State Electrolyte for Long-Cycle-Life Rechargeable Zinc–Air Batteries, ACS Sustain Chem Eng. 11 (2023) 3732–3739. https://doi.org/10.1021/acssuschemeng.2c06661.

[97] G.M. Wu, S.J. Lin, C.C. Yang, Alkaline Zn-air and Al-air cells based on novel solid PVA/PAA polymer electrolyte membranes, J Memb Sci. 280 (2006) 802–808. https://doi.org/10.1016/j.memsci.2006.02.037.

[98] C.-C. Yang, S.-J. Lin, S.-T. Hsu, Synthesis and characterization of alkaline polyvinyl alcohol and poly(epichlorohydrin) blend polymer electrolytes and performance in

electrochemical cells, J Power Sources. 122 (2003) 210–218. https://doi.org/10.1016/S0378-7753(03)00429-4.

[99] X. Fan, J. Liu, Z. Song, X. Han, Y. Deng, C. Zhong, W. Hu, Porous nanocomposite gel polymer electrolyte with high ionic conductivity and superior electrolyte retention capability for long-cycle-life flexible zinc–air batteries, Nano Energy. 56 (2019) 454–462. https://doi.org/10.1016/j.nanoen.2018.11.057.

[100] O. Kwon, H.J. Hwang, Y. Ji, O.S. Jeon, J.P. Kim, C. Lee, Y.G. Shul, Transparent Bendable Secondary Zinc-Air Batteries by Controlled Void Ionic Separators, Sci Rep. 9 (2019) 3175. https://doi.org/10.1038/s41598-019-38552-4.

[101] S.S. Shinde, C.H. Lee, J.-Y. Yu, D.-H. Kim, S.U. Lee, J.-H. Lee, Hierarchically Designed 3D Holey C_2N Aerogels as Bifunctional Oxygen Electrodes for Flexible and Rechargeable Zn-Air Batteries, ACS Nano. 12 (2018) 596–608. https://doi.org/10.1021/acsnano.7b07473.

[102] C.-C. Yang, S.-J. Lin, Alkaline composite PEO–PVA–glass-fibre-mat polymer electrolyte for Zn–air battery, J Power Sources. 112 (2002) 497–503. https://doi.org/10.1016/S0378-7753(02)00438-X.

[103] Q. Liu, Y. Wang, L. Dai, J. Yao, Scalable Fabrication of Nanoporous Carbon Fiber Films as Bifunctional Catalytic Electrodes for Flexible Zn-Air Batteries, Advanced Materials. 28 (2016) 3000–3006. https://doi.org/10.1002/adma.201506112.

[104] A.A. Mohamad, Zn/gelled 6M KOH/O2 zinc–air battery, J Power Sources. 159 (2006) 752–757. https://doi.org/10.1016/j.jpowsour.2005.10.110.

[105] Z. Li, M. Shao, Q. Yang, Y. Tang, M. Wei, D.G. Evans, X. Duan, Directed synthesis of carbon nanotube arrays based on layered double hydroxides toward highly-efficient bifunctional oxygen electrocatalysis, Nano Energy. 37 (2017) 98–107. https://doi.org/10.1016/j.nanoen.2017.05.016.

[106] M. Yu, Z. Wang, C. Hou, Z. Wang, C. Liang, C. Zhao, Y. Tong, X. Lu, S. Yang, Nitrogen-Doped Co_3O_4 Mesoporous Nanowire Arrays as an Additive-Free Air-Cathode for Flexible Solid-State Zinc-Air Batteries, Advanced Materials. 29 (2017) 1602868. https://doi.org/10.1002/adma.201602868.

[107] S. Qu, Z. Song, J. Liu, Y. Li, Y. Kou, C. Ma, X. Han, Y. Deng, N. Zhao, W. Hu, C. Zhong, Electrochemical approach to prepare integrated air electrodes for highly stretchable zinc-air battery array with tunable output voltage and current for wearable electronics, Nano Energy. 39 (2017) 101–110. https://doi.org/10.1016/j.nanoen.2017.06.045.

[108] Y. Li, C. Zhong, J. Liu, X. Zeng, S. Qu, X. Han, Y. Deng, W. Hu, J. Lu, Atomically Thin Mesoporous Co_3O_4 Layers Strongly Coupled with N-rGO Nanosheets as High-Performance Bifunctional Catalysts for 1D Knittable Zinc–Air Batteries, Advanced Materials. 30 (2018) 1703657. https://doi.org/10.1002/adma.201703657.

[109] X. Zhu, H. Yang, Y. Cao, X. Ai, Preparation and electrochemical characterization of the alkaline polymer gel electrolyte polymerized from acrylic acid and KOH solution, Electrochim Acta. 49 (2004) 2533–2539. https://doi.org/10.1016/j.electacta.2004.02.008.

[110] J. Fu, J. Zhang, X. Song, H. Zarrin, X. Tian, J. Qiao, L. Rasen, K. Li, Z. Chen, A flexible solid-state electrolyte for wide-scale integration of rechargeable zinc–air batteries, Energy Environ Sci. 9 (2016) 663–670. https://doi.org/10.1039/C5EE03404C.

[111] C. Guan, A. Sumboja, H. Wu, W. Ren, X. Liu, H. Zhang, Z. Liu, C. Cheng, S.J. Pennycook, J. Wang, Hollow Co_3O_4 Nanosphere Embedded in Carbon Arrays for Stable and Flexible Solid-State Zinc-Air Batteries, Advanced Materials. 29 (2017) 1704117. https://doi.org/10.1002/adma.201704117.

[112] Y. Yang, T. Wang, Y. Guo, P. Liu, X. Han, D. Wu, Agar-PVA/GO double network gel electrolyte for high performance flexible zinc-air batteries, Mater Today Chem. 29 (2023) 101384. https://doi.org/10.1016/j.mtchem.2023.101384.

[113] T.M. Di Palma, F. Migliardini, D. Caputo, P. Corbo, Xanthan and κ-carrageenan based alkaline hydrogels as electrolytes for Al/air batteries, Carbohydr Polym. 157 (2017) 122–127. https://doi.org/10.1016/j.carbpol.2016.09.076.

[114] Y. Wang, R. Liu, W. Chen, W. Li, W. Zheng, H. Zhang, Z. Zhang, Bimetallic Sulfides Embedded in a Boron Modulated Carbon Matrix as the Bifunctional Catalyst with a Low Oxygen Evolution Reaction Overpotential for an Advanced Zinc-Air Battery, ACS Sustain Chem Eng. 10 (2022) 14486–14494. https://doi.org/10.1021/acssuschemeng.2c03971.

[115] J. Fu, F.M. Hassan, J. Li, D.U. Lee, A.R. Ghannoum, G. Lui, Md.A. Hoque, Z. Chen, Flexible Rechargeable Zinc-Air Batteries through Morphological Emulation of Human Hair Array, Advanced Materials. 28 (2016) 6421–6428. https://doi.org/10.1002/adma.201600762.

[116] D. Jiang, H. Wang, S. Wu, X. Sun, J. Li, Flexible Zinc–Air Battery with High Energy Efficiency and Freezing Tolerance Enabled by DMSO-Based Organohydrogel Electrolyte, Small Methods. 6 (2022) 2101043. https://doi.org/10.1002/smtd.202101043.

[117] Y. He, W. Shang, M. Ni, Y. Huang, H. Zhao, P. Tan, In-situ observation of the gas evolution process on the air electrode of Zn-air batteries during charging, Chemical Engineering Journal. 427 (2022) 130862. https://doi.org/10.1016/j.cej.2021.130862.

[118] Z. Song, J. Ding, B. Liu, Y. Shen, J. Liu, X. Han, Y. Deng, C. Zhong, W. Hu, Investigation of failure mechanism of rechargeable zinc–air batteries with poly(acrylic acid) alkaline gel electrolyte during discharge–charge cycles at different current densities, Chemical Engineering Journal. 429 (2022) 132331. https://doi.org/10.1016/j.cej.2021.132331.

[119] M. Wang, N. Xu, J. Fu, Y. Liu, J. Qiao, High-performance binary cross-linked alkaline anion polymer electrolyte membranes for all-solid-state supercapacitors and flexible rechargeable zinc–air batteries, J Mater Chem A Mater. 7 (2019) 11257–11264. https://doi.org/10.1039/C9TA02314C.

[120] N. Zhao, F. Wu, Y. Xing, W. Qu, N. Chen, Y. Shang, M. Yan, Y. Li, L. Li, R. Chen, Flexible Hydrogel Electrolyte with Superior Mechanical Properties Based on Poly(vinyl alcohol) and Bacterial Cellulose for the Solid-State Zinc–Air Batteries, ACS Appl Mater Interfaces. 11 (2019) 15537–15542. https://doi.org/10.1021/acsami.9b00758.

[121] D. Lee, H.-W. Kim, J.-M. Kim, K.-H. Kim, S.-Y. Lee, Flexible/Rechargeable Zn–Air Batteries Based on Multifunctional Heteronanomat Architecture, ACS Appl Mater Interfaces. 10 (2018) 22210–22217. https://doi.org/10.1021/acsami.8b05215.

[122] M.J. Tan, B. Li, P. Chee, X. Ge, Z. Liu, Y. Zong, X.J. Loh, Acrylamide-derived freestanding polymer gel electrolyte for flexible metal-air batteries, J Power Sources. 400 (2018) 566–571. https://doi.org/10.1016/j.jpowsour.2018.08.066.

[123] Q. Liu, C. Xia, C. He, W. Guo, Z.P. Wu, Z. Li, Q. Zhao, B.Y. Xia, Dual-Network Structured Hydrogel Electrolytes Engaged Solid-State Rechargeable Zn-Air/Iodide Hybrid Batteries, Angewandte Chemie. 134 (2022). https://doi.org/10.1002/ange.202210567.

[124] W. Li, W. Chen, H. Zhang, Z. Zhang, Integratable solid-state zinc-air battery with extended cycle life inspired by bionics, Chemical Engineering Journal. 435 (2022) 134900. https://doi.org/10.1016/j.cej.2022.134900.

[125] J. Béjar, L. Álvarez–Contreras, F. Espinosa–Magaña, J. Ledesma–García, N. Arjona, L.G. Arriaga, Zn–air battery operated with a 3DOM trimetallic spinel

(Mn0.5Ni0.5Co2O4) as the oxygen electrode, Electrochim Acta. 391 (2021) 138900. https://doi.org/10.1016/j.electacta.2021.138900.

[126] A.R. Mainar, J.A. Blázquez, D. Frattini, M. Enterría, N. Ortiz-Vitoriano, I. Urdampilleta, H.-J. Grande, High performance carbon free bifunctional air electrode for advanced zinc-air batteries, Electrochim Acta. 446 (2023) 142075. https://doi.org/10.1016/j.electacta.2023.142075.